Bogdan Molchanov

Experimental Validation of Spray Deflectors' Impact on Performance of High-Speed Planing Craft

School of Engineering

Thesis submitted for examination for the degree of Master of Science in Technology.

Espoo 04.10.2018

Thesis supervisor:

Jani Romanoff, DSc

Thesis advisors:

Mirjam Fürth, PhD

Karl Garme, PhD

Aalto University
School of Engineering

Aalto University
School of Engineering

Aalto University, P.O. Box 11000
00076, AALTO
www.aalto.fi

Abstract of master thesis

Author Bogdan Molchanov

Title of Thesis Experimental Validation of Spray Deflectors' Impact on Performance of High-Speed Planing Craft

Master programme Nordic Master in Maritime Engineering **Code** ENG214

Thesis supervisor Jani Romanoff

Thesis advisors Mirjam Fürth and Karl Garme

Date 04.10.2018 **Number of Pages** 52 + 21 **Language** English

Abstract

High-speed planing craft is designed to overcome conventional hull's speed barrier associated with wave making resistance and high frictional forces. Despite being able to reach high speeds, some planing hull forms will develop large volumes of spray attached to the hull surface, which can account for a large proportion of the total resistance.

In this study, an experimental evaluation of the novel spray deflector technology proposed by Petestep AB is carried out in model scale at the Davidson Laboratory towing tank. The spray deflectors are compared against a time-proven spray rails technology and bare hull configuration. A modular hull design was developed that allows for rapid conversion between the three hull configurations and for future modifications to the design.

The calm water resistance tests have shown up to 9% resistance reduction for spray rails and up to 25.75% reduction for spray deflectors as compared to the bare hull configuration. The running position of the spray deflector configuration was affected by the selected deflector design and differed from the spray rail and bare hull configuration, making the direct comparison of the technologies inapplicable. The irregular waves tests have shown that for the current deflector design, the significant accelerations are approximately the same for the spray rail and spray deflector configurations. Both the technologies have led to increased accelerations at the center of gravity as compared to the bare hull. The spray deflector configuration, however, experienced lower accelerations in the bow area. A number of improvements to the current model design were proposed for the next series of experiments.

Keywords Spray resistance, planing hull, Savitsky method, model scale, towing tank, spray rails, spray deflectors, high-speed craft

ACKNOWLEDGMENTS

I would like to thank Chiara Wielgosz for creating this project opportunity and giving me a helping hand with relocation to the US and initiation of the thesis work.

I am profoundly grateful to be part of the team with Dr. Mirjam Fürth, Svante Lundmark and Mathew Green. This was enjoyable and productive work atmosphere and I will miss working with you greatly. I would also like to thank Dr. Raju Datla, Professor Michael DeLorme, Uihoon Chung and Douglas Meding for your patience and providing us with practical and theoretical support when we needed it the most.

My sincere thanks to Professors Jani Romanoff and Karl Garme for agreeing to be my academic advisors. Your feedback was always thought provoking and contributed greatly to the quality of this work.

Special thank you to Arcada Stipendiefonder's and Aalto Exchange grant committees for seeing potential in this project and making my travel and stay financially possible.

Last but not least, I would like to thank all my friends and family for supporting me and being with me spiritually during my studies. I especially thank my girlfriend for staying supportive and patient with all the traveling I had to do during the past two years.

Bogdan Molchanov

New Jersey, September 2018

TABLE OF CONTENTS

ABBREVIATIONS AND SYMBOLS

Acronyms

CFD	Computational Fluid Dynamics
HSC	High-Speed Craft
ITTC	International Towing Tank Conference
LCG	Longitudinal Centre of Gravity
RANS	Reynolds Averaged Navier-Stokes equation
SLR	Speed to Length Ratio $\left[Knots/\sqrt{ft} \right]$
VCG	Vertical Centre of Gravity

Greek Symbols

α	The angle between keel and stagnation line $[deg]$
β	Deadrise angle of the hull $[deg]$
ε	Thrust inclination relative to the keel $[deg]$
θ	The angle between spray edge and keel $[deg]$
λ	Mean wetted length to beam ratio $[-]$
$\Delta\lambda$	Increase in λ due to spray $[-]$
Δ	Hull displacement $[N]$
∇	Displaced volume by the hull $[m^3]$
ρ	Water density $[kg/m^3]$
τ	The trim angle between the keel and still water surface $[deg]$
ν	The kinematic viscosity of the fluid $[m^2/s]$
μ	Scaling factor

Symbols

a	Lever arm between R_f and VCG $[m]$
A_{wetted}	Wetted surface of the hull $[m^2]$
A_{spray}	Area wetted by whisker spray $[m^2]$
A_{dry}	The area in contact with air projected on a vertical plane $[m^2]$
B	A beam of the hull $[m]$
c	Lever arm between the center of pressure C_p and LCG $[m]$
C	Length of stagnation line $[m]$
C_A	Aerodynamic drag coefficient $[-]$
C_F	Skin friction coefficient $[-]$

$C_{L\beta}$	Lift coefficient of a hull with deadrise $[-]$
C_{Lo}	Lift coefficient of a flat plate $[-]$
C_p	Center of pressure on the hull bottom $[m]$
C_R	Residual resistance coefficient $[-]$
C_T	Total resistance coefficient $[-]$
C_v	Beam Froude number $[-]$
f	Lever arm between the thrust axis and VCG $[m]$
Fn	Froude number $[-]$
Fn_∇	Volumetric Froude number $[-]$
g	Acceleration due to gravity $[m/s^2]$
H	The measured rise of VCG in planing regime $[m]$
L_c	Chine wetted length $[m]$
L_k	Keel wetted length $[m]$
L_m	Mean wetted length $[m]$
L_{wave}	Wave length $[m]$
L_{wl}	Waterline length $[m]$
L_{ws}	Characteristic length of whisker spray $[m]$
N	Normal force on the hull bottom due to pressure $[N]$
R_{air}	Aerodynamic resistance $[N]$
R_e	Reynolds number $[-]$
R_f	Frictional resistance $[N]$
R_I	Induced pressure resistance $[N]$
R_s	Spray resistance $[N]$
R_T	Total resistance $[N]$
T	Thrust applied $[N]$
V_{hull}	The speed of the hull $[m/s]$
V_m	Average flow speed under the hull bottom $[m/s]$
V_{wave}	The speed of wave propagation $[m/s]$

LIST OF FIGURES

LIST OF TABLES

1. INTRODUCTION

High-speed planing craft has been experiencing a significant increase in demand and applications in recent decades. With applications ranging from small recreational power boats to search and rescue and military craft, the improvements in performance are being constantly sought after.

The most essential feature of the planing craft is the ability to attain relatively high speeds with limited engine power. A lot of research effort is focused on possibilities of reducing planing hull's resistance to minimize fuel consumption at design speeds.

Typically, the reduction in resistance is achieved by minimizing the wetted area of the hull by either lifting it out of the water or by splitting the wetted area into multiple smaller areas through the use of a step, an abrupt change of the keel depth at some point along the hull bottom.

An alternative solution proposed by a Swedish company, Petestep AB, reduces planing hull's resistance by minimizing area wetted by spray above the water level. An example of spray associated with planing is shown in Figure 1. The technology uses spray deflectors, that are said to catch and reflect spray backward, thus reducing frictional drag and converting some of the spray's kinetic energy into forward thrust. In addition, the spray deflector design is expected to reduce vertical accelerations experienced by craft and crew in waves, thus increasing the level of the crew's comfort and safety. (Bjersten and Danielsson, 2014)

The spray deflectors are expected to be an improvement of the spray rails technology that also works by detaching spray from the hull's surface but deflecting it sideways rather than backward. (Clement, 1964)

Figure 1. Search and rescue boat surrounded by spray (Swedeship AB, 2018)

1.1. RESEARCH GAP

Although spray deflection technologies have been around for at least 60 years, little research attention was given to the spray phenomenon. The spray rails design proposed by Clement (1964) is widely used by the industry but "rules of thumb" are still used for estimation of their impact on vertical accelerations experienced by hull in rough seas and it was not until recently that prediction method was developed for estimation of spray resistance in calm water (Eliasson and Larsson, 2000; Savitsky et al., 2007).

Petestep spray deflector solution has received some academic attention. A numerical study was performed by Olin et. al (2016), which showed promising results of up to 28% reduction in drag and about 4% gain in the forward thrust when compared to bare bottom setup. A follow up experimental evaluation of the numerical study by Wielgosz et. al (2018) had concluded the experimental setup to be physically infeasible to reproduce in model scale.

Another study by Wielgosz (2018) was performed for a hull ex-novo, where resistance and vertical accelerations results were compared in model scale between hull with bare bottom and hull fitted with Petestep deflectors. The experiments showed up to 12.1% reduction in resistance and up to 10.8% reduction in bow accelerations.

With limited theoretical background about the flow properties of the spray and scarce empirical and numerical data for spray rails and deflectors, additional benchmark tests are required to draw conclusions on the efficiency of the Petestep deflector design.

1.2. OBJECTIVES

The aim of this research is to develop a hull model suitable for comparison of three hull bottom configurations – bare hull, hull with spray rails and hull with Petestep deflectors – and to conduct series of model tests for comparison of total resistance in calm water and accelerations in waves.

The work is comprised of multiple milestones. The first step is to design a hull that would generate spray forces of high magnitude. The intention is to have a high proportion of spray force relative to total resistance, so that spray deflection technologies can be effectively compared. The three hull configurations should have the same mass, scale, shape, and center of gravity for direct comparison of the results. The first milestone is then formulated as

"To design hulls or a modular hull suitable for benchmarking in calm water and irregular waves tests and that would generate spray forces constituting a significant proportion of the total resistance"

The next milestone is to develop a test matrix and test procedure that would yield meaningful and accurate results. This involves uncertainty management, the design of speed matrix and experimental setup that would fit into time schedule allocated by the towing tank facility. The second milestone is therefore

"To design experimental setup and speed matrix for benchmarking of the three hull bottom configurations in calm water and in irregular waves tests."

The final milestone is to carry out a series of experiments and do post-processing and analysis of the results. The comparison will focus on showing and comparing the efficiency of the selected spray deflection technologies. Finally, improvements for further study will be proposed based on the acquired knowledge. The final milestone is then

"To carry out resistance and accelerations experiments for the three hull bottom configurations, identify the efficiency of the Petestep deflectors technology and propose further research direction."

1.3. WORK DIVISION

This thesis work was done in collaboration with Svante Lundmark, a graduate student from the Royal Institute of Technology. Both authors shared an equal level of involvement for all the stages of this project. Although responsibilities varied slightly, the final decisions were revised jointly until approval of both participants.

Achieving the first milestone was the primary responsibility of Bogdan. The work included the design of the three hull configurations and physical set up of the experiments.

Svante was responsible for the second milestone, which involved the design of the speed matrix, compliance with International Towing Tank Conference (ITTC) rules and documentation of the test procedures.

The final milestone of organizing, postprocessing and interpreting the results was done jointly.

2. LITERATURE REVIEW

2.1. INTRODUCTION TO HIGH SPEED PLANING CRAFT

2.1.1. CONVENTIONAL HULL'S SPEED LIMIT

At slow speeds, the weight of the ship is supported by predominantly hydrostatic forces according to Archimedes' principle and the hydrodynamic drag is governed by frictional forces. As the speed increases, the water flow around the hull starts to create pressure forces that can no longer be neglected. These forces are directly related to the wave pattern along the hull – creating suction in the throughs and lift in the crests. The relationship between wave's length L_{wave} and speed of its propagation V_{wave} is (Molland et al., 2011)

$$V_{wave}/\sqrt{gL_{wave}} = 0.4 \quad (1)$$

This relationship is also known as Froude number or F_n. For ships, the waterline length L_{wl} is constant, so at a certain speed V_{hull} the length of waterline and wave becomes the same

$$\frac{V_{hull}}{\sqrt{gL_{wl}}} = \frac{V_{wave}}{\sqrt{gL_{wave}}} = 0.4 \quad (2)$$

This is the theoretical wave barrier for conventional displacement hulls. When the wave barrier is approached, hull develops significant bow-up trim and negative pressure distribution along the entire hull bottom leading to a rise in displacement and drag.

As seen from equation (2) theoretical maximum speed increases with the length of the ship. Another option is to increase power and reduce the weight of the hull through use of lightweight materials and light motors. This combination leads to increased running trim angles makes it easier for the hull to climb on top of its own bow wave. A more elegant solution to overcome speed limit, however, is to design hull shape such that entire hull bottom acts as a lifting surface.

2.1.2. CHARACTERISTICS OF PLANING HULLS

The planing craft has characteristic V-shaped hulls that are designed to overcome wave making a barrier at high speed. They are typically characterized by transom stern, flat buttock lines and hard chines. A typical body plan is shown in Figure 2. The hull generates lift from hydrodynamic forces, which at high speeds trim the forepart of the hull out of the water. Thus, at high speeds, the hull reduces its wetted area and therefore reduces frictional and wave making drag (Eliasson and Larsson, 2000). Figure 3 demonstrates a parabolic relationship between drag and Froude number for conventional hull shapes. Planing hulls follow parabolic relationship until $Fn{\sim}0.4$, where dynamic lift starts to dominate, leading to rise of the vertical center of gravity (VCG) and decreased wetted area (Rosén, 2004).

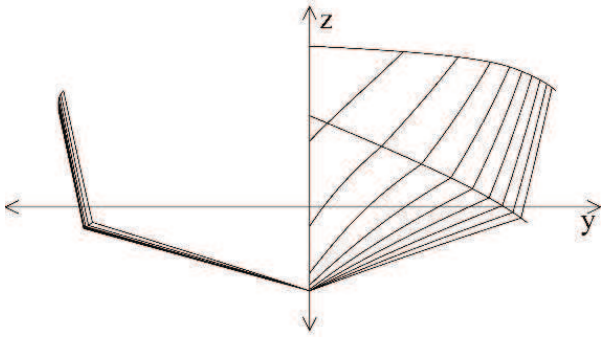

Figure 2. An example of planing craft hull shape

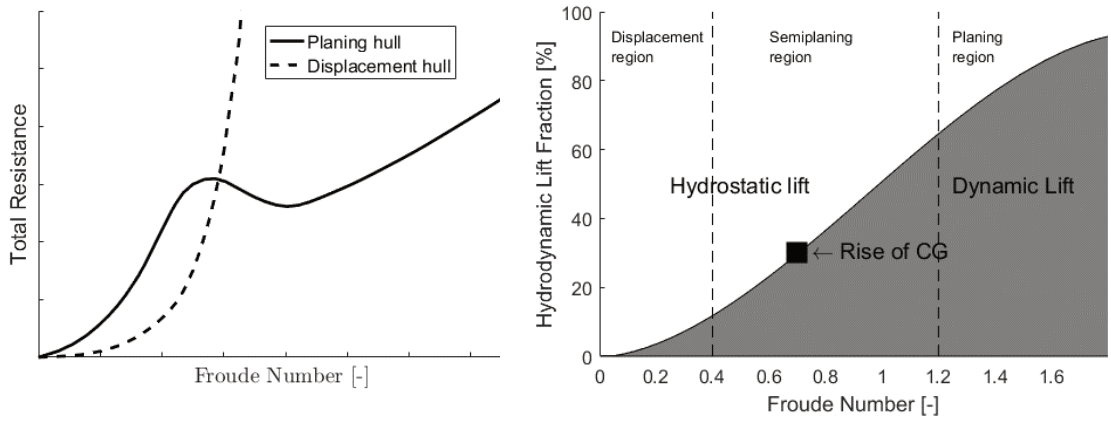

Figure 3. Schematics. Left: F_n– drag relationship for conventional and planing hulls (Rosén, 2004); Right: Proportion of dynamic lift vs F_n (Eliasson and Larsson, 2000)

Early planing craft theory was based on resistance theories for seaplanes and addressed by researchers such as Sambraus (1938), Shoemaker (1934) and Sottorf (1934). The empirical theory based on previously gathered data and systematic tests for flat plates and prismatic hulls was formulated by Savitsky (1964). Savitsky Method is widely used nowadays, generally with corrections and additions from later research, and is based on the hull geometry, forces equilibrium and running position of the craft.

The equilibrium position is defined by trim angle τ and wetted area of hthe ull, which are both functions of speed and hull shape. The schematic drawing of high speed craft's running position is shown in Figure 4 (Molland et al., 2011). A more thorough discussion about forces acting on the hull is given in Section 2.3.

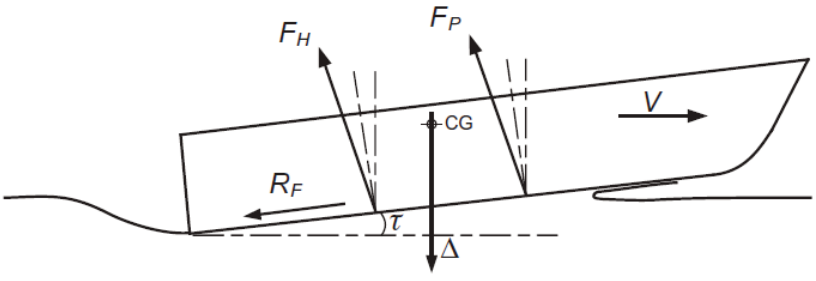

Figure 4. Running position and main forces acting on the hull at planing speeds (Molland et al., 2011)

2.2. EXPERIMENTAL BACKGROUND

2.2.1. HYDRODYNAMIC RESISTANCE COMPONENTS

This section is intended to give a general overview of hull resistance. An example breakdown of resistance components reproduced from Larsson and Raven (2010, pp. 13–15) for various hull forms is shown in Figure 5. Each bar corresponds to 100% of total resistance.

For planing craft, wave breaking does not really happen. Instead, spray forces become significant at planing speeds. The appendages (shown in red) are also of importance for planing craft as they greatly increase wetted surface area, while the form effects are negligible when the bow is out of the water.

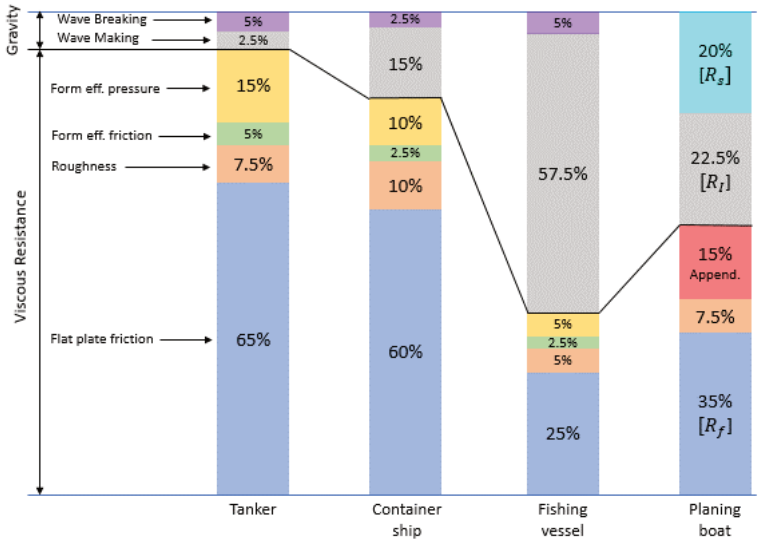

Figure 5. Breakdown of resistance for different hull types (Larsson and Raven, 2010)

The general breakdown of resistance components is shown in Figure 6. The blue color highlights resistance components important for planing craft. The actual relationships between resistance components shown in the graph are more complex and covered more thoroughly in (Molland et al., 2011, pp. 14–17).

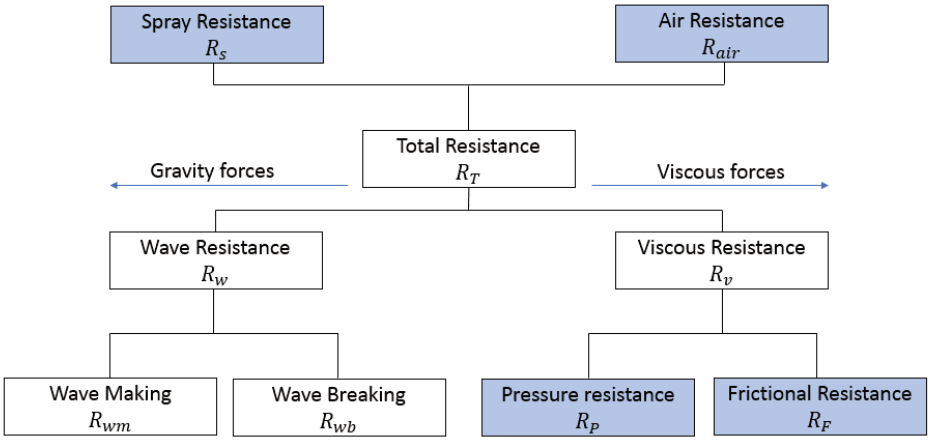

Figure 6. A simplified breakdown of resistance components (Molland et al., 2011)

The frictional resistance $\boldsymbol{R_f}$ shown in Figure 4 arises from friction between hull surface and water due to local deceleration of flow and formation of the boundary layer. The major part of the fluid around the hull behaves as inviscid and its velocity is independent of the hull's speed. In near proximity of the hull's surface, however, flow is dominated by viscous effects, making water particles move along with hull surface. This layer is called the boundary layer. Due to change of fluid velocities across the boundary layer, shear stresses arise. Summation of the shear stresses over the entire wetted surface of the hull yields frictional resistance. The change of fluid's velocity profile over the boundary layer is shown in Figure 7.

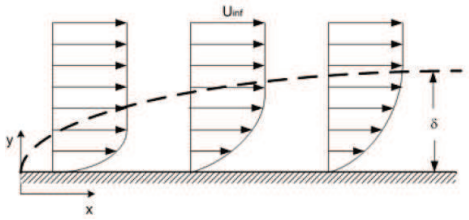

Figure 7. Change of fluid velocity profile between the 2D surface and inviscid flow (Molland et al., 2011)

Viscous pressure resistance $\boldsymbol{R_p}$ arises due to viscosity and the hull form. As the hull moves forward, it pushes the water in the direction of its own propagation. Therefore, normal stresses arise over the wetted surface due to varying flow velocity around the hull. Summation of those stresses over the surface yields the pressure resistance. For planing hull, the dynamic pressure and buoyancy forces (Figure 4) are broken up into vertical and horizontal components. Vertical component is the lift force is responsible for planing phenomenon while horizontal component is called induced drag $\boldsymbol{R_I}$ (Savitsky, 1964)

$$R_I = \Delta tan\tau \tag{3}$$

Horizontal force component grows in proportion to trim angle and thus lower trim angles are associated with more efficient planing.

Another major contributor to ship's resistance is wave making $\boldsymbol{R_w}$. The pressure distribution around moving ship causes free surface to rise in regions of high pressure and fall in regions of low pressure, generating systems of transverse and divergent almost stationary waves, when considered in relative motion with the ship. The bow and stern waves' interference is a function of hull's speed causing variation in wetted area and pressure distribution around the hull.

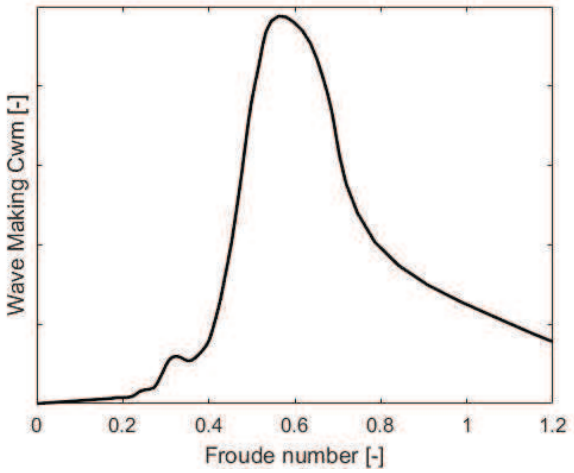

Figure 8. Approximate representation of wave-making resistance coefficient as a function of Froude number

Wave making resistance, therefore, increases with Froude number but has "humps" and "hollows" due to wave interferences. Recalling equation (2) at $F_n = 0.4$ the theoretical speed limit for the conventional hull is reached. At this speed, the dynamic pressure will push planing hull on top of its own bow wave as shown in Figure 4. Wave making resistance starts to rapidly decrease as waterline length rapidly becomes smaller than the generated wave length. Schematic representation of dependence of wave making resistance on the speed of planing craft is shown in Figure 8. The figure was made by combining the wave making coefficients of a displacement hull ($Fn \in 0\text{: } 0.5$) and of a planing hull ($Fn \in 0.5\text{: } 1.2$).

In terms of hydrodynamics, high-speed craft (HSC) are designed to overcome wave making resistance R_w and to diminish frictional resistance R_f. Due to significant trim angles at initial planing speeds induced pressure resistance R_I is significant. The aerodynamic resistance R_{air} becomes significant at high planing speeds. Also, it was shown that for some combinations of hull forms and trim angles resistance due to spray R_s can become a significant part of the total resistance (Savitsky et al., 2007). A more thorough discussion on calculation of resistance components for planing craft is given in the following sections.

2.2.2. MODEL PARAMETER SCALING

Prior to building a new vessel or implementing new technology, its performance is usually investigated using numerical or experimental methods. To reduce costs, experiments are done to scale. This allows for precise control of the environment and low risks compared to full scale experiments. Experiments require careful planning as scaling of measured quantities is not a straightforward task. Extrapolation of model test data gives insight into full scale hull resistance as well as its running position, accelerations and generated wave patterns.

For accurate prediction, the main dimensions of the model should be a scale factor μ smaller than the full-scale design as shown in equation (4) for geometrical similarity.

$$\begin{bmatrix} L_{model} \\ B_{model} \\ T_{model} \end{bmatrix} \times \mu = \begin{bmatrix} L_{design} \\ B_{design} \\ T_{design} \end{bmatrix}$$
$$\beta_{model} \quad = \quad \beta_{design} \tag{4}$$
$$\nabla_{model} \times \mu^3 = \nabla_{design}$$

Where L, B, T, β & Δ are length, beam, draft, deadrise angle and displacement of the hull respectively. Keeping similitude between dimensions as well as weight distribution ensures that wetted surface A_w will be of the same shape in both model and full scale.

In addition to that, kinematic and dynamic similarities must be fulfilled. This means that velocities, forces and masses must also follow the scaling laws. As shown in Figure 6, to ensure similarity between measured hydrodynamic forces the gravity, pressure and viscous forces need to be the same in the model and full scale.

Euler number $\boldsymbol{E_u}$ is responsible for the similarity of pressure forces. This number is generally important for cavitation experiments.

Froude number $\boldsymbol{F_n}$ similarity ensures correct scaling of gravity forces. Gravity forces play a dominant role in wave resistance and correct wave pattern forming. Therefore, Froude

number is an important factor for surface ships. In the following equations, subscript M refers to model scale and S refers to full scale (Molland et al., 2011).

$$F_n = \frac{V_M}{\sqrt{g \cdot L_M}} = \frac{V_S}{\sqrt{g \cdot L_S}}$$
$$V_M = \frac{V_S}{\sqrt{\mu}} \tag{5}$$

Reynold's number $\boldsymbol{R_e}$ similarity yields correct scaling of viscous forces. Reynold's number influences all hydrodynamic components to some extent since water is not completely inviscid. Reynold's number depends on the viscosity of fluid ν in which the ship will operate (Molland et al., 2011).

$$R_e = \frac{V_M \cdot L_M}{\nu_M} = \frac{V_S \cdot L_S}{\nu_S}$$
$$V_M = V_S \cdot \mu \cdot \frac{\nu_M}{\nu_S} \tag{6}$$

As seen from equations (5) and (6), it is impossible to satisfy both Reynold's and Froude similarity at the same time. Froude law of scaling is used for model tests of surface ships because it allows testing models at slower speeds in model scale than in full scale. (Molland et al., 2011)

Scaling is also often used for easier comparison of the results between different hulls and research groups. The choice of scaling method depends on practices of the industry branch. Currently the research groups typically use volumetric Froude number for presenting resistance tests results (De Marco et al., 2017; Kim et al., 2013; Kohansal and Ghassemi, 2010; Lotfi et al., 2015).

The volumetric Froude number $\boldsymbol{Fn_\nabla}$ is defined as

$$Fn_\nabla = \frac{V_{hull}}{\sqrt{g \times \sqrt[3]{\nabla}}} \tag{7}$$

2.2.3. MODEL SCALE TESTING

Dimensional analysis is a common approach to solving problems of complex nature in engineering. The approach of the dimensional analysis is to bring all the parameters within the equation to the same dimensional space. This is achieved by expressing both sides of the equation in terms of basic physical quantities – mass, length and time (M, L, t). (Bertram, 2000)

For instance, the ship's total resistance R can be constructed. The ship is propagating at constant speed V and has characteristic length L. It generates waves that are a governed by gravitational acceleration g. Finally, the hull is in contact with water, the properties of which are defined by its density ρ and kinematic viscosity ν. The parameters all have a varying effect on the hull resistance, which is considered by writing relation in the power form (Bertram, 2000)

$$R \propto \rho^a V^b L^c \nu^d g^e \tag{8}$$

The quantities in equation (8) are brought into the same dimensional space expressing everything as basic physical quantities

$$\frac{ML}{T^2} \propto \left(\frac{M}{L^3}\right)^a \left(\frac{L}{T}\right)^b L^c \left(\frac{L^2}{T}\right)^d \left(\frac{M}{T^2}\right)^e \tag{9}$$

Solving for coefficients of equation (9) the following relationship is obtained

$$\frac{R}{\rho V^2 L^2} = f(\frac{VL}{v}, \frac{gL}{V^2}) \tag{10}$$

Total resistance is shown to be a function of F_n and R_e previously shown in equations (5) and (6). The right-hand side is the nondimensional resistance coefficient. The L^2 the parameter is dimensionally the same as the wetted area A_w, which is preferred for comparison of geometrically similar hulls. This lays a foundation for the model scale testing and extrapolation of results to full scale as described further. The method is following guidelines of the International Towing Tank Conference, ITTC (1957).

First, the bare model hull resistance R_{TM} is measured in the towing tank. Then the force is represented as a nondimensional coefficient

$$C_{TM} = \frac{R_{TM}}{0.5\rho V_M^2 A_{wM}} \tag{11}$$

Total resistance C_{TM} is assumed to be composed of frictional resistance C_{FM} and residual resistance C_{RM}.

$$C_{TM} = C_{FM} + C_{RM} \tag{12}$$

The frictional resistance coefficient is dependent on Reynold's number and therefore must be estimated both for the model and full scale using ITTC-57 model-ship correlation line

$$C_{Fi} = \frac{0.075}{(logR_{ei} - 2)^2} \tag{13}$$

Where $R_{eM}$and R_{eS} are calculated using equation (6). The residual resistance coefficient of the model is assumed to follow Froude scaling law, therefore

$$C_{RM} = C_{RS} = C_R = C_{TM} - C_{FM} \tag{14}$$

The full-scale resistance coefficient is then calculated as

$$C_{TS} = C_{FS} + C_R + C_A \tag{15}$$

Where C_A is typically a correction factor, which comes from the experience of the towing tank testing and compensates for roughness allowance and errors from measurement devices. Finally, the total resistance is

$$R_{TS} = 0.5\rho V_S^2 A_{wS} C_{TS} \tag{16}$$

For HSC, the situation is slightly different, since its resistance can be taken as a sum of friction, induced pressure, spray and air resistance coefficients.

$$C_{TM} = C_{FM} + C_{IM} + C_{SM} + C_{AirM} \tag{17}$$

The frictional resistance is found using equation (13). Induced resistance as seen from equation (3) depends on the displacement and trim angle, so it follows Froude scaling law. The spray drag follows Reynold's scaling law. Savitsky et al (2007) highlight that area wetted by spray has local friction coefficient and provides a method for finding its estimate.

2.3. PREDICTION OF PLANING CRAFT'S PERFORMANCE

The theory in the following sections is based on the theoretical and experimental results of the publications presented in Table 1. This list also shows state of the art of spray deflection technologies. Some of the listed publications are discussed more thoroughly in sections 2.3.1-2.4.2.

Table 1. List of significant publications related to spray phenomenon

Author	Type of study	Significant results (for spray area)
(Wagner, 1932)	Theoretical model	2D case - spray thickness estimation
(Sottorf, 1934)	Experimental (model)	Observations of generated spray and its experimental height measurements
(Parkinson, 1935)	Experimental (model)	Side by side pictures of observed spray patterns in the model tests
(Locke and Bott, 1943)	Experimental (model)	A method of rapid measurements of spray shape from photographs
(Pierson, 1950)	Theoretical	An update to calculation of spray thickness
(Kapryan and Boyd, 1953)	Experimental (model) and Analytical	Systematic tests with vertical chine stripes – effects on lift and drag
(McBride, 1956)	Experimental (model)	Correlation of lift and drag exerted by spray on a "wing" to scale of the model
(Savitsky and Breslin, 1958)	Experimental (model) and Analytical	Origin and shape of the main and whisker spray. 2D spray thickness equation
(Clement, 1964)	Experimental (model)	Used short and long spray rails to reduce total resistance.
(Payne, 1982)	Theoretical	Volumetric flow of spray and multiple cases for spray thickness calculations
(Latorre, 1983)	Experimental (model)	In-situ measurement of spray thickness and flow state in spray area
(Latorre and Ryan, 1989)	Experimental (model)	Found scale/speed limits where break up of spray blister into droplets occurs
(Kihara, 2006)	Numerical	2D+T simulation of nonlinear surface flow around the hull including spray
(Savitsky et al., 2007)	Semi-empirical & theoretical	An update to Savitsky (1964) method – including spray and air drag forces
(Lee et al., 2010)	Experimental/Numerical	Use of spray rails for semi-planing hull shapes
(Savitsky and Morabito, 2011)	Experimental/Analytical	Prediction and measurement of spray trajectory and geometry

(Seo et al., 2016)	Experimental (model)	Use of spray rails to manipulate Center of Pressure, trim and lift of planing hull
(Olin et al., 2016)	Numerical	Evaluation of spray deflectors and validation of spray thickness equations
(Wielgosz et al., 2018)	Experimental (model)	Experimental validations of results by Olin et al. (2016)
(Wielgosz, 2018)	Experimental (model)	Comparison of calm water resistance and accelerations in waves between bare hull and hull with spray deflectors

2.3.1. PLANING OF FLAT SURFACES

One of the initial theoretical models for flat planing surfaces was developed by Wagner (1932) and later used as the foundation of the Savitsky Method (1964). The simplest 2D case of planing surface is a flat plate as shown in Figure 9.

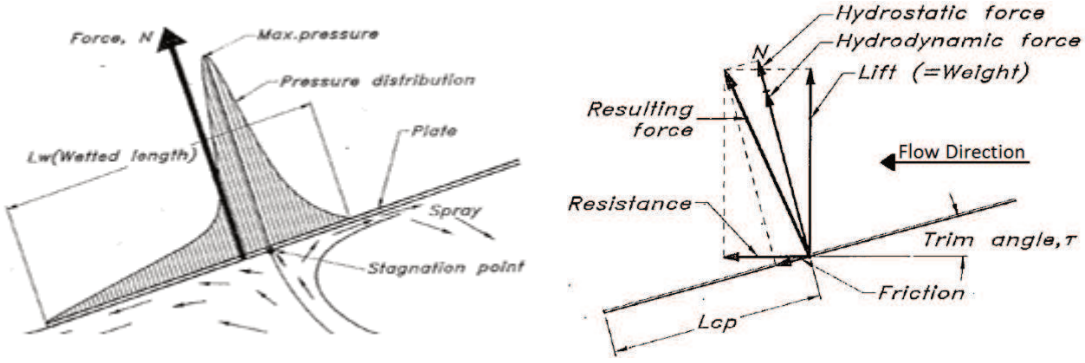

Figure 9. Left: pressure force distribution for planing flat plate; Right: forces acting on a planing plate (Savitsky, 1964)

The fluid velocity vectors show how the flow propagates relatively to the plate surface. At the plate's trailing edge flow is almost parallel to the plate's surface. Further in at some point along the plate, the flow hits the plate at a right angle. This location is known as the stagnation point. The area between the stagnation point and the trailing edge is called a wetted or pressure area. At the stagnation point, the pressure reaches its maximum since there is no flow relative to the plate and all kinematic energy of the fluid is converted into pressure forces (Eliasson and Larsson, 2000).

Forward of the stagnation point, the flow is redirected forward in the form of a spray. In the equilibrium condition, shown on the right-hand side of Figure 9, the plate is propagating at a constant trim angle τ relative to the calm water surface. The dynamic and static pressures are represented as the resultant normal force acting through the center of pressure. The vertical component of the resultant force is the lifting force that counteracts the plate's weight. The horizontal component of the resultant force is the induced drag R_I introduced in equation (3).

2.3.2. PLANING OF PRISMATIC HULLS

Although a flat surface is an efficient way to develop dynamic lift, it comes at a penalty of high accelerations in waves. A V-shape is a more practical solution for the majority of applications since according to Allen and Jones (1972) and Razola et al. (2014) magnitude of the impact's load on the hull bottom decreases for increasing deadrise angles.

Due to the deadrise angle, flow under the hull bottom develops the transversal component. Since the fluid is moving sideward, the pressure on the hull becomes lower than on a flat plate of equivalent area. Therefore, the lift force decreases with increasing deadrise angle. On the other hand, during impact V-shaped hull immerses gradually into a wave, leading to a significant reduction in accelerations (Eliasson and Larsson, 2000).

Savitsky (1964) has established an empirical relationship between the lift coefficient of a flat plate and prismatic hull with constant deadrise angle. Central terminology required for implementation of Savitsky Method is presented further. An example calculation is presented in (Eliasson and Larsson, 2000, p. 192; Savitsky, 1964, p. 89).

2.3.3. KEY DEFINITIONS OF EMPIRICAL MODEL

The following section explains the key definitions and equations 18-23 found in the Savitsky (1964) Method and will be used throughout the study. Some of the definitions are shown in Figure 10.

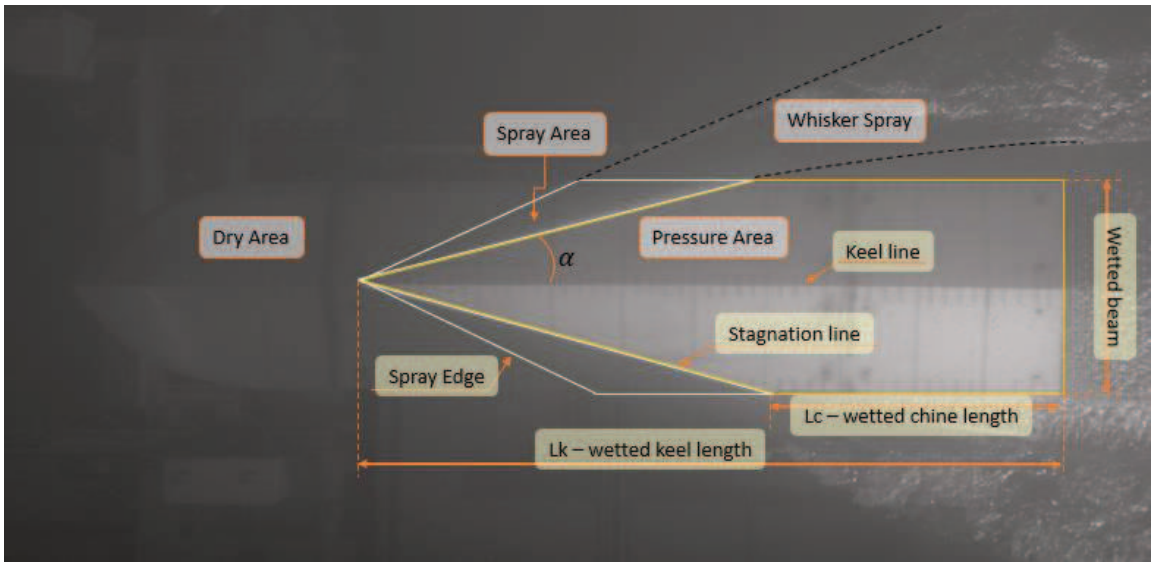

Figure 10. Key elements of the planing hull's bottom

For planing hulls, the only geometrical parameter that does not vary significantly with speed is wetted beam $\boldsymbol{b}$, so it is used for scaling purposes. The wetted beam is the width of the planing surface [m]. Generally, the beam is measured between chines but in some cases, the distance between spray rails can be taken if the chines run dry. The chines are flat surfaces with sharp corners that effectively detach flow from hull sides.

Another geometrical parameter is deadrise angle $\boldsymbol{\beta}$ [deg] formed between the hull's bottom and horizontal plane. The deadrise facilitates flow to the sides and decreases impact accelerations. To get a positive pressure distribution throughout the hull bottom,

flow separation is also required at the sides of the hull. This is typically achieved by having chines.

The speed coefficient $\boldsymbol{C_v}$ or beam Froude number is used to scale forces and speeds, since the beam is the only constant length.

$$C_v = \frac{V}{\sqrt{gb}} \tag{18}$$

A hull underway will attain equilibrium trim angle $\boldsymbol{\tau}$, measured between the keel line and the waterplane at which the summation of all the forces acting on the hull becomes zero.

When planing, most of the hull's own weight is supported by hydrodynamic forces. The nondimensional lift coefficient $\boldsymbol{C_{L\beta}}$ of a hull is

$$C_{L\beta} = \frac{\Delta}{0.5\rho V^2 b^2} \tag{19}$$

Since Savitsky Method is based on a flat plate, the lift coefficient of the hull with the deadrise needs to be converted into $\boldsymbol{C_{Lo}}$, the lift of the hull with the same displacement but without deadrise.

$$C_{L\beta} = C_{Lo} - 0.0065\beta C_{Lo}^{0.6} \tag{20}$$

When the hull is trimmed, the water plane intersects both the keel line and the chines. The distances measured from the transom to the intersection of waterplane with the keel and the chines are defined as $\boldsymbol{L_k}$ and $\boldsymbol{L_c}$ respectively (Figure 10). The arithmetic average of L_c and L_k is called mean wetted length, used for finding wetted area.

$$L_m = \frac{L_k + L_c}{2} \tag{21}$$

A dimensionless measure of wetted length is the wetted length to beam ratio $\boldsymbol{\lambda}$. This is a central geometrical parameter for defining the wetted area and the center of pressure.

$$\lambda = L_m/b \tag{22}$$

During initial design, however, L_c and L_k values are not known, so λ is found through iteration of equation (23)

$$C_{Lo} = \tau^{1.1}(0.012\lambda^{0.5} + 0.055\frac{\lambda^{2.5}}{C_v^2}) \tag{23}$$

2.3.4. PRESSURE (WETTED) AREA

The hull bottom of the craft can be divided into three distinct flow areas when planing, usually referred to as pressure area, spray area and dry area. The areas are marked in Figure 10. The equations 24-28 follow the original Savitsky (1964) publication.

The pressure or wetted area is the lift generating surface of the hull. This area carries all pressure forces and is the backbone of the planing phenomenon. The normal force is acting through the center of pressure $\boldsymbol{C_p}$ defined as

$$C_p = L_m(0.75 - \frac{1}{\frac{5.21C_v^2}{\lambda^2} + 2.39}) \tag{24}$$

The lever arm $\boldsymbol{c}$ between C_p and longitudinal centre of gravity (LCG) is

$$c = LCG - C_p L_m \tag{25}$$

The frictional resistance of the hull projected on the keel plane is found according to standard ITTC (2002) guidelines

$$R_F = \rho V_m^2 A_p C_F = \rho V_m^2 \lambda b^2 C_F \tag{26}$$

Where C_f is the skin friction coefficient, which can also be found in ITTC (2002) . The V_m is the average flow velocity over the hull bottom with a deadrise calculated as

$$V_m = V\sqrt{1 - \frac{C_{L\beta}}{\lambda cos\tau}} \tag{27}$$

And wetted area A_p is calculated as

$$A_p = L_m b/cos\beta \tag{28}$$

2.3.5. STAGNATION LINE AND SPRAY EDGE

The stagnation line is located at the forward edge of the pressure area. At the stagnation line, the pressure on the hull reaches its maximum since there is almost no flow relative to the hull and all kinetic energy of the fluid is converted into pressure. A relationship for the angle between the stagnation line and the keel in the horizontal plane is given by Savitsky (1964, pp. 72–74)

$$\alpha = \text{atan}\frac{\pi\ tan\tau}{2\ tan\beta} \tag{29}$$

The $\pi/2$ multiplier is called pile up factor. For planing hull at speed, the wetted length extends slightly further from the location of stagnation line due to the build-up of water. Olin et al. (2016) highlights that although $\pi/2$ is a widely accepted value, the actual pile up factor varies slightly as a function of trim and deadrise.

From α the length of the stagnation line C and the angle of the spray edge θ are (Savitsky et al., 2007)

$$C = \frac{b/2}{Sin\alpha} \tag{30}$$

$$\theta = 2\alpha \tag{31}$$

2.3.6. WHISKER SPRAY AREA

The spray area located between the stagnation line and the spray edge is formed by incident flow reflected forward from the stagnation line. Since the spray is in contact with the hull, there is frictional resistance present in the spray area. Therefore, the whisker spray causes an increase in the wetted area.

Clement (1964) hypothesized that total resistance can be reduced by detaching flow from hull's spray area. He showed that by use of sharp-edged stripes applied in the spray area and running parallel to keel a reduction of up to 18% in resistance is possible. Clement's experimental set up is sketched in the top half-hull of the Figure 11. These stripes (drawn in red) are now referred to as spray rails, commonly used in HSC to deflect spray sideways.

An analytical model for prediction of volumetric flow and energy lost in a transversal component of whisker spray was presented by Payne (1982). He concluded that wave making resistance becomes negligible in planing regions while spray resistance increases.

Latorre and Ryan (1989) analysed the difference between the model and the full scale spray. In model scale spray appears as a blister but as the scale increases the spray starts to break up into droplets. This phenomenon is attributed to the surface tension of water and inertia forces. This work has produced a method of predicting scale and speed limit for a prismatic hull where break up of blister into droplets occurs.

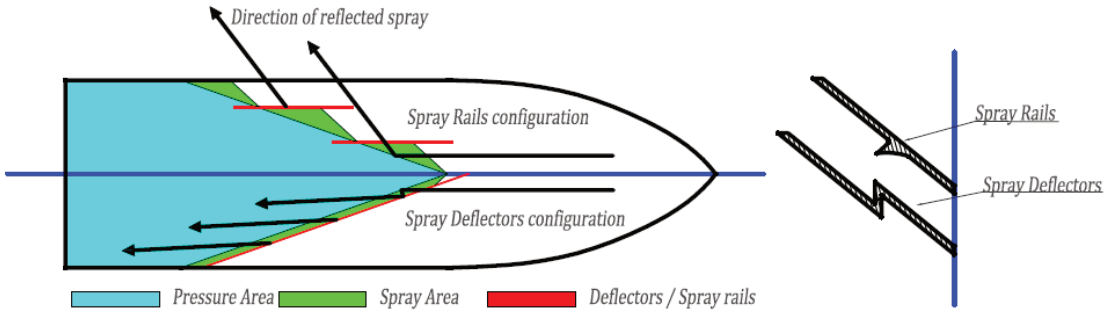

Figure 11. Left: Comparison of spray flow between spray rail and spray deflector; Right: Cross-sectional view of spray rail and spray deflector (Olin et al., 2016)

Finally, the method of predicting the spray area, its contribution to total drag and design guidelines for locating spray rails were published by Savitsky et al. (2007). Authors concluded that surface tension in the spray sheet has a negligible impact on friction drag. The published guidelines are additions to the Savitsky (1964) method. The below presented definitions and equations 32-34 are introduced by Savitsky et al. (2007).

When whisker spray is considered as a part of the wetted area, the mean wetted length to beam ratio λ increases by a factor of $\boldsymbol{\Delta\lambda}$. The magnitude of $\Delta\lambda$ is dependent on hull geometry and running position

$$\Delta\lambda = \frac{Cos\theta}{4\,Sin\theta \times Cos^2\beta} \tag{32}$$

This relation indirectly shows that small trim angle and high deadrise angle will maximize whisker spray resistance. The dependency of $\Delta\lambda$ on deadrise and trim is presented in Savitsky et al. (2007, fig. 4). The viscous resistance $\boldsymbol{R_S}$ in the spray area is

$$R_S = \frac{1}{2}\rho V^2\,\Delta\lambda b^2 C_S \tag{33}$$

The C_S is local friction coefficient in the whisker spray. Additional discussion about flow state in the spray is presented in Appendix A

2.3.7. Dry Frontal Area

The dry area forward of the spray edge does not interact with the water and only contributes to the aerodynamic resistance, $\boldsymbol{R_{air}}$. The contribution from aerodynamic resistance was determined by towing hulls in the air at zero-degree trim. The air drag is calculated as

$$R_{air} = \frac{1}{2}\rho_{air} V^2 A_{dry} C_{Air} \quad (34)$$

Drag coefficient $\boldsymbol{C_{Air}}$ of a typical bow shape is approximately 0.7 (Savitsky et al., 2007).

2.3.8. DYNAMIC FORCE-MOMENT EQUILIBRIUM

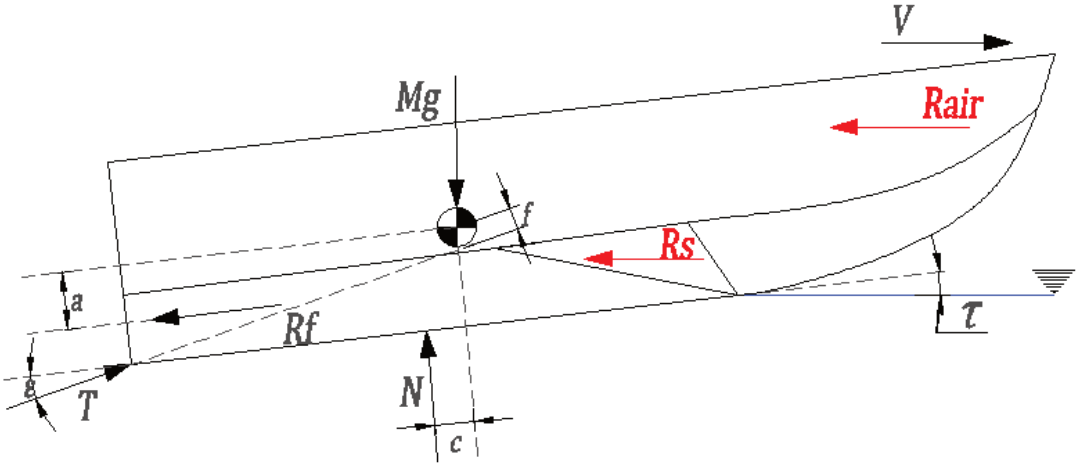

Figure 12. Schematic of forces acting on HSC in a dynamic equilibrium (Savitsky, 1964; Savitsky et al., 2007)

Figure 12 represents the equilibrium of forces and moments acting on the hull. In order to compute to equilibrium trim angle, the remaining lever arms need to be defined.

The thrust force $\boldsymbol{T}$ is applied at the location of the propeller hub and is aligned at an angle $\boldsymbol{\varepsilon}$ measured between thrust axis (propeller shaft) and the keel line. The thrust axis passes at a distance $\boldsymbol{f}$ from the VCG. Usually, ε and f are defined by the designer. Equations 35-39 are following Savitsky (1964)

The lever arm $\boldsymbol{a}$ is formed between frictional resistance resultant and VCG and is calculated from the hull geometry

$$a = VCG - \frac{B}{4}\tan\beta \quad (35)$$

With all the forces known and lever arms defined, equilibrium equations can be constructed. The vertical equilibrium is

$$\Delta = N cos\tau + T sin(\tau + \varepsilon) - R_f sin\tau \quad (36)$$

The horizontal equilibrium is

$$T cos(\tau + \varepsilon) = R_f cos\tau + N sin\tau \quad (37)$$

The moment equilibrium is

$$Nc + R_f a - Tf = 0 \quad (38)$$

By rearranging the equations (36)-(38) and assuming that $\varepsilon = 0$, which is the case for present study, the equilibrium equation becomes (Savitsky, 1964, p. 91)

$$\Delta[c \times cos\tau - f sin\tau] + R_f(a - f) = 0 \quad (39)$$

Through iterations of equation (39) the equilibrium trim angle of the hull can be found. In the Savitsky et al. (2007) method, the Savitsky (1964) method is used to calculate equilibrium trim angle and resistance. The spray and aerodynamic resistances (R_s and

R_{air} shown in red in Figure 12) are then added to calculated pressure and friction resistances

$$R_{tot} = R_f + R_I + R_s + R_{air} \quad (40)$$

2.4. DEFLECTION OF WHISKER SPRAY

2.4.1. SPRAY RAILS

Use of spray rails is a popular way to improve lift and reduce the drag of the hull. The spray rails run longitudinally along the hull and have sharp edges that facilitate effective flow separation from the spray area. As seen from Clement's (1964) results, the spray rails are the most effective in the spray area, while inclusion of the spray rails behind the stagnation line could result in an increase in drag. Spray rails redirect spray sideways and downward reducing wetted area and increasing dynamic lift. Approximately 88% of the whisker spray can be deflected using short spray rails (Savitsky et al., 2007).

As of now, there is no well-defined way of including lift from spray rails into Savitsky method. A rough approach mentioned by Eliasson and Larsson (2000) suggests taking a deadrise angle between the keel and the tip of the spray rail rather than along the hull surface. This results in smaller deadrise angle and hence higher theoretical lift and accelerations. If the craft's chines are running dry, the beam is measured between the spray rails.

The transversal location of the spray rails is suggested to be roughly at 25, 50 and 75% of the half beam outboard of the keel. Preferred cross section of spray rail is triangular with a sharp outer edge to promote flow separation (Eliasson and Larsson, 2000, fig. 10.10).

2.4.2. SPRAY DEFLECTORS

Although spray rails are effective means of separating spray sideways there still is room for improvements. As stated above, spray rails can effectively detach about 88% of the spray, meaning there remains some spray attached to the hull. The spray is redirected sideways whereas it could be redirected backward to gain additional thrust for the hull. Finally, relatively flat spray rail surfaces are responsible for increased accelerations in rough seas (Eliasson and Larsson, 2000, p. 194).

A novel approach to deflection of spray was patented by Petestep AB company (Bjersten and Danielsson, 2014). The deflector is placed at a slight offset along the stagnation line and is incorporated as part of the hull bottom structure as opposed to spray rails that can be retrofitted. This arrangement is expected to redirect spray aftward and downward. The downward component of redirected spray should contribute to additional lift while the aftward component should generate additional thrust. Deflectors are expected to further reduce wetted area compared to spray rails and therefore reduce frictional drag (Bjersten and Danielsson, 2014). A comparison between the flow behavior and the cross sections of the rails and deflector is shown in Figure 11. The thick black arrows show the direction of the reflected spray flow for both rail and deflector configurations.

An initial numerical study of the spray deflectors' performance was done by Olin et al (2016). CFD study was done for a 3D-flow case for prismatic wedge hulls with constant

deadrise angle between 10 and 30 degrees. The authors used the Volume of Fluid, VOF, method based on Reynolds averaged Navier-Stokes (RANS) and on $k-\omega$ Shear Stress Transport. The study concluded that, comparing to bare hull running in the same equilibrium condition, up to 32% reduction in total resistance is possible. Reduction of 28% is associated with the diminished wetted surface area in the spray region and an additional 4% was gained from aftward reflection of spray.

An attempt to validate results from Olin et al (2016) through model tank testing was done by (Wielgosz et al., 2018). The model was fixed in heave and trim to mimic the running condition used by Olin et al. The experiments concluded numerical model to be infeasible for physical evaluation at least in model scale.

To further investigate the performance of the spray deflectors, a model with deflectors incorporated into the hull bottom was experimentally tested and compared to the bare hull (Wielgosz, 2018). In the new experimental setup, the model was free to heave and trim. It was noted that due to different force equilibrium for the hull fitted with LCG must be moved to achieve the same running condition as for the bare hull. Reduction in the total resistance of up to 12.1% was achieved for cases where the stagnation line was slightly aft of the deflectors. It was also found that vertical accelerations were reduced by up to 10.8% at the bow in irregular waves.

2.5. HIGH-SPEED CRAFT IN WAVES

Most of the methods described in preceding sections are given for calm water scenario. For practical applications, a compromise needs to be made between calm water design and seakeeping performance of craft in waves.

A systematic study of various hull shapes and loading conditions was done and summarized by Fridsma (1969). Prior to this, designers would rely upon their own experience and very limited test data, usually for specific hull forms. Fridsma (1969) ran series of tests for hulls with varying deadrise angles with hydrodynamic bow shapes but prismatic after-bow hull forms. In addition, the effect of the beam to length ratio was investigated for a 20-degree deadrise hull. The outcome of this study was later included by Savitsky & Brown (1976) in the form of equations rather than graphs and tables.

One of the outcomes of the experiments is the prediction method for the added resistance in waves. The formula is based on speed to length ratios (SLR)

$$SLR = \frac{V}{\sqrt{L_{wl}}} \left[\frac{Knots}{\sqrt{ft}}\right] \tag{41}$$

Added resistance formula is readily available only for SLR of 2, 4 and 6 and needs to be interpolated for the other speeds. The hull behavior in these three speed regimes is different. According to Savitsky and Brown (1976) at low speed ranges the motion amplitudes are generally the highest because the hull tends to follow the wave profile. At medium speeds, added resistance due to waves reaches its maximum. Finally, at high speeds, the accelerations experienced by the hull are at its highest. The paper concludes that in order to avoid severe accelerations the trim angle and the length to beam ratio (L_{wl}/B) should be kept low while the deadrise and the craft's inertia should be increased.

One example of practical applications of these findings is the DNV-GL (2015) rules for the design of HSC. This rule chapter is intended specifically to take into account expected

rough-weather conditions and ensure structural safety and safety of crew on board. The safety is increased by voluntary reduction of speed in heavy weather. The crew is advised to stay below certain speed limits, which are a function of significant wave height (H_s) and properties of the hull. Typical voluntary speed restriction curve is as shown in Figure 13.

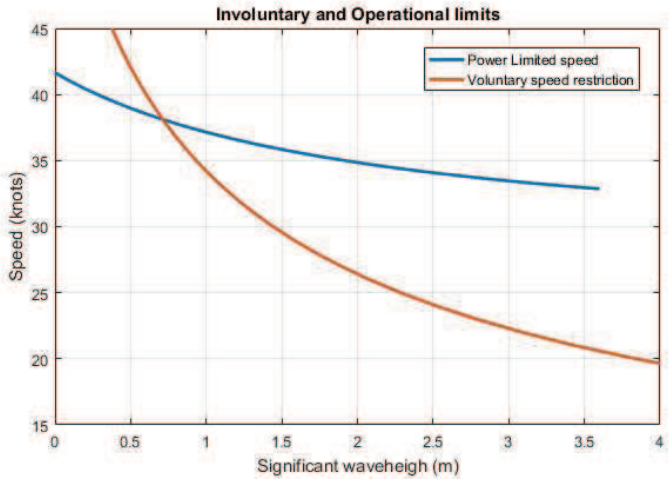

Figure 13. An example speed-sea state curve. Blue: reduction in maximum speed due to added resistance in waves. Orange: Voluntary reduction of speed due to high impact accelerations

3. METHODOLOGY

This chapter addresses the development of a model for towing tank testing. The first section focuses on the development of a model for the proposed research that satisfies all given constraints. The second section provides detail design for the selected model dimensions. Finally, the third section introduces experimental set up for calm and rough water tests.

3.1. MODEL DESIGN

In this project, a novel model is designed with the purpose of answering two research questions. The first goal is to test whether the spray deflectors are more efficient than the spray rails in minimizing total resistance. The second goal is to compare vertical accelerations experienced by the three hull configurations in irregular waves. All of the experiments are conducted at the same model scale with the same geometry, displacement and weight distribution to allow for accurate and direct comparison.

3.1.1. REQUIRED HULL CONFIGURATIONS

To effectively compare spray rail and spray deflector configurations, baseline data is required. Bare hull will, therefore, act as a baseline for resistance and spray rails for acceleration data comparison as shown in Table 2.

Table 2. Two hull setups and their expected performance vs bare hull performance

Hull type:	Bare Hull	Spray Rails	Spray Deflectors
Geometry and mass	Baseline	Same	Same
Total Resistance	Baseline	Lower (Clement, 1964)	Lowest (Assumption)
Impact accelerations	Lower (Assumption)	Baseline	Unknown

3.1.2. SPRAY AREA REQUIREMENT

Both the rail and the deflector technologies reduce total resistance through diminishing spray area and redirection of the flow. The hull needs to be designed in a way that would give high magnitude of spray resistance so that the difference with and without spray is significant. From equation (32) it is seen that spray area factor $\Delta\lambda$ is maximized for combinations of low trim and high deadrise angles. Equation (33) shows how the magnitude of the spray resistance depends on the speed and width of the hull. The magnitude of the spray resistance R_S is thus an important design parameter and must be higher than the measurement error. A more thorough discussion on sizing the model to maximize the spray resistance is given in Appendix A.

The contribution of spray resistance to total resistance is another important parameter of the study. In order to accurately measure and compare the effects of spray rails or deflectors, the contribution from the spray area to the total resistance needs to be as high as possible. To achieve this, the trim angle needs to be as low as possible to minimize induced drag and maximize spray resistance.

Another important parameter to aim for is the state of flow in the spray area. The spray will account for a larger part of the total resistance when the flow in the spray area changes from laminar to transitional. More information on the subject is provided in Appendix A.

3.1.3. DESIGN LIMITATIONS

The model design was constrained to several physical and project limitations such as towing tank parameters, manufacturing processes and time. The discussion about constraints is summarized in Table 3.

Towing tank limitations
The towing tank at the Davidson Laboratory is 95.40 m long, 5.00 m wide with a variable depth from 1.98 to 2.29 meters. The maximum constant towing speed is 18.30 m/s, but it is generally not operated at speeds above 11 m/s for safety reasons. The tests can be carried out in calm water or in regular or irregular waves. The maximum wave height is ~0.61 m.

According to ITTC (2002), the model length has to be at least 2 times smaller than the tank width and at least 0.8 times smaller than the tank depth to avoid blockage and interference effects. This results in a limit of 2.45 m on the maximum model length. Model length is also limited by the maximum carriage speed. As seen from equation (5), since the maximum speed is limited, longer models will have lower maximum Froude number than shorter models. Finally, the model displacement was limited by the tank operators to 50 Lb (~22.7 kg) in the wave tests to avoid damaging the hull and the equipment.

Material and manufacturing limitations
Majority of the newer models in the towing tank are made in-house from marine grade Divinycell Foam. According to the foam suppliers, the blocks come in $48 \times 96''$ size ($1.22 \times 2.44\ m$) with custom thickness. The density of foam can be selected from 10, 15 or 20 Lb/ft^3. In this case, higher density means higher model weight and cost but also higher mechanical strength and higher quality of surface finish. The toolpaths require at least $1''$ (2.54 cm) offset from the hull surface, effectively limiting the model to ~2.39 meters in maximum length.

Spray area limitations
As spray resistance is a central topic of this study, the design is aiming to maximize spray contribution to model resistance. First of all, for higher spray magnitude, the flow in the spray area needs to be in the transitional state. Discussion in Appendix A shows that all of the main dimensions of the model as well as selected speeds affect the flow state in the spray area. This limitation can be used as a minimum requirement for model dimensions and speed. The magnitude and the relative contribution of the spray forces are being maximized in this study. It was decided to place a minimum aim of 1 N for theoretical spray magnitude and at least 5% contribution to total resistance. This was done to make sure that results between hull configurations are not significantly affected by measurement error.

Table 3. Table of design limitations

Towing tank limitations		Comments
Maximum speed	$V_{max} = 11\ m/s$	Limits F_n_max
Towing tank dimensions	Tank width: $L_m < 2.5\ m$	ITTC (2002)
	Tank depth: $L_m < 2.475\ m$	
Displacement	$\Delta < 22.7\ kg$	For equipment safety
Manufacturing limitations		Comments
Block size and tool paths	$L_m < 2.37\ m$	Allowance for tool paths
Foam density	$\Delta < 22.7\ kg$	Impacts model cost and weight
Spray area limitations		Comments
Transitional flow state	$R_{eS} > 1.5 \times 10^6$	Appendix A
Spray force magnitude	$R_S > 1\ N$	To minimize error
Spray force contribution	$\frac{R_S}{R_{total}} \geq 5\ \%$	To validate technology

3.1.4. DESIGN CONCEPT

The shape of the hull is the first step in the design spiral. Possible hull shapes that were considered as parent models for the project are listed in Table 4.

The final choice was to take the model from Wielgosz (2018) as a parent hull but to simplify the hull geometry so that it aligns closely with Savitsky empirical model. In this way, the Savitsky method is accurate for deciding on locations and geometry of the spray rails and deflectors and predicting bare hull performance while parent hull serves as a reference for the expected results and aids in final dimension selection.

The hull is therefore prismatic from the transom stern up until the furthest intersection between the stagnation line and the keel line. The bow was formed to have reasonable hydrodynamic properties for pre-planing speed ranges and wave tests. Thus, in calm water tests immersed part of the hull would be only prismatic, removing uncertainties associated with non-prismatic hull shapes.

The hull shape from Clement (1964) was not selected due to low deadrise angle, which would result in high impact accelerations in the wave tests. Both hulls from Clement (1964) and Petestep (2016) are non-prismatic and have quite low L/B ratio, which are not beneficial for this study. More discussion on effects of L/B ratios is given in Section 3.1.6.

Table 4. Options considered for the parent hull model

Hull Form	(Clement, 1964)		
Particulars	$\beta = 12°$	$L_{wl}/B = [3.06,4.09]$	Curved hull
Advantages	Data exists for bare hull and for spray rails (calm water)		
Disadvantages	Deadrise too low for wave tests; Hull is not prismatic		
Hull Form	(Fridsma, 1969)		
Particulars	$\beta = 20°$	$L_{wl}/B = [4,5,6]$	Prismatic
Advantages	Acceleration data can be compared directly to reference for a broad range of L_{wl}/B ratios. Prismatic body and easy to reproduce bow shape		
Disadvantages	Bow shapes used in this study were of elliptical form, so measured bow accelerations might be higher than with the conventional bow design.		
Hull Form	(Savitsky, 1964)		
Particulars	Suitable for a broad range of dimensions		Prismatic
Advantages	Simple hull shape, leading to a high accuracy of empirical formulas. Allows to predict the design location of deflectors and spray rails		
Disadvantages	Bow shapes not suitable for wave tests. Although the empirical formulas work well, the experimental data does not cover the entire spectrum of L_{wl}/B ratios and deadrise angles		
Hull Form	(Wielgosz, 2018)		
Particulars	$\beta = 20°$	$L_{wl}/B = 4.67$	Mostly Prismatic
Advantages	The only model that has experimental data for bare spray deflectors for calm water and irregular waves. Drawings are readily available saving production and planning time		
Disadvantages	In order for results to be comparable, deflectors need to have same cross section and placement as in reference. The flow state in reference work was laminar, so scaling of spray resistance will produce errors.		
Hull Form	(Petestep AB, 2016)		
Particulars	$\beta = 22.8°$	$L_{wl}/B = 3.3$	Curved hull
Advantages	Drawings exist for bare hull and hull with steps. Full scale data available for comparison		
Disadvantages	Complex hull shape, making results harder to interpret and predict		

3.1.5. MODULAR HULL DESIGN

Once the prismatic hull shape had been chosen, several solutions for how to manufacture the models were proposed. One requirement was to test at least two deflector pairs. Each pair was to be tested separately from the other to minimize uncertainty in the results.

The conversion from the bare hull to spray rail set up can be done by attaching spray rail strips to the hull using glue or double-sided tape (Clement, 1964). Deflectors, on the other hand, require modification to the hull bottom geometry for each pair. This leads to three setups: bare hull/spray rail hull and two spray deflector hull setups. A mind map of possible solutions to the bottom structure is shown in Figure 14.

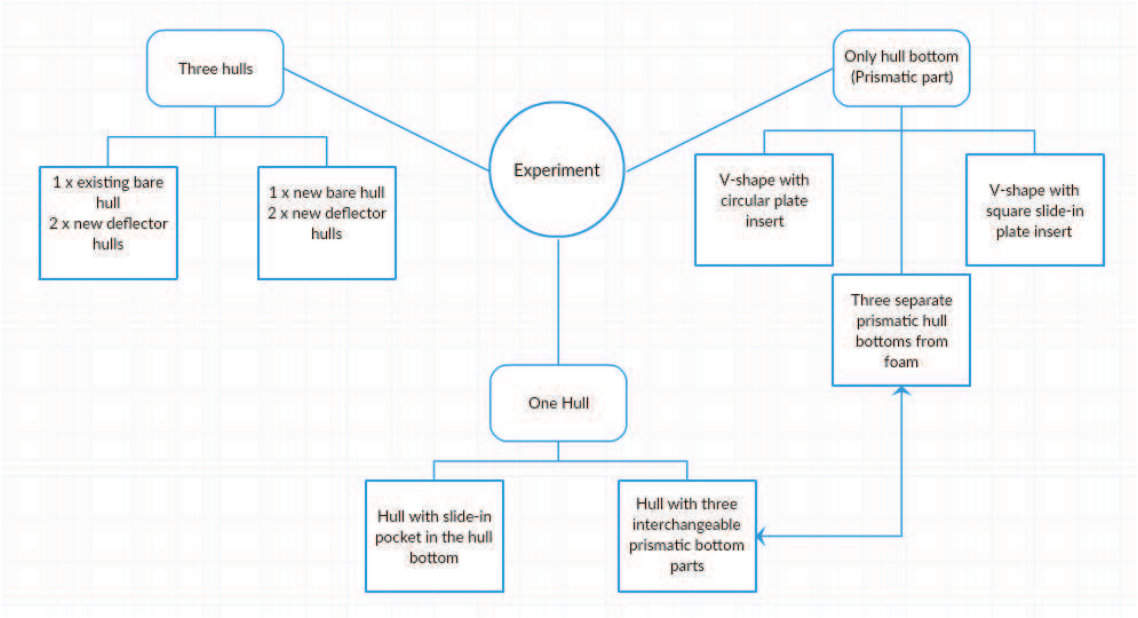

Figure 14. Mindmap of hull design options

Most of the ideas were ruled out early in the study because they would not satisfy all of the criteria. Three or two full hulls, for instance, would lead to high material and production costs along with the requirement to switch models between testing and recalibration of equipment. The purely prismatic hull would yield the lowest investment costs, but the study would be limited only to calm water tests and in predefined fixed trim and heave condition. The final two concepts are shown in Figure 15. The white part is the detachable bottom.

Figure 15. Top: a concept with the interchangeable prismatic bottom; Bottom: a concept with interchangeable flat plate insert

The design with plastic plate inserts (bottom of Figure 15) is cheaper, faster to manufacture and gives sharper edge on the deflector. In addition, the hull bottom always remains watertight and is structurally stronger than the concept with detachable bottom (top of Figure 15).

The detachable bottom, on the other hand, would make it possible to vary the L/B ratio of the hull. The plastic insert design was selected since it would give the opportunity to test multiple deflector pairs in the future at low costs.

3.1.6. LENGTH TO BEAM RATIO

As mentioned by Clement '*the potential gain from use of the spray rails is greater for relatively short wide hull than for a relatively long narrow hull*' (Clement, 1964, p. 4).

This observation is true for the friction force magnitude in the spray. On the other hand, the relative contribution of spray drag to total drag is higher for slender hull. This assumption was verified in Matlab by fixing model's speed and selecting L/B ratio of 4 as a starting point. The initial dimensions of the model were chosen such that flow in the spray area is in the transitional state for all tested cases.

First, length was varied, and beam was fixed and then beam was varied and length was fixed. In this way, a spectrum of L/B ratios were covered as shown in Figure 16. The displacement and the LCG of the model were scaled according to Froude scaling law to ensure results are comparable.

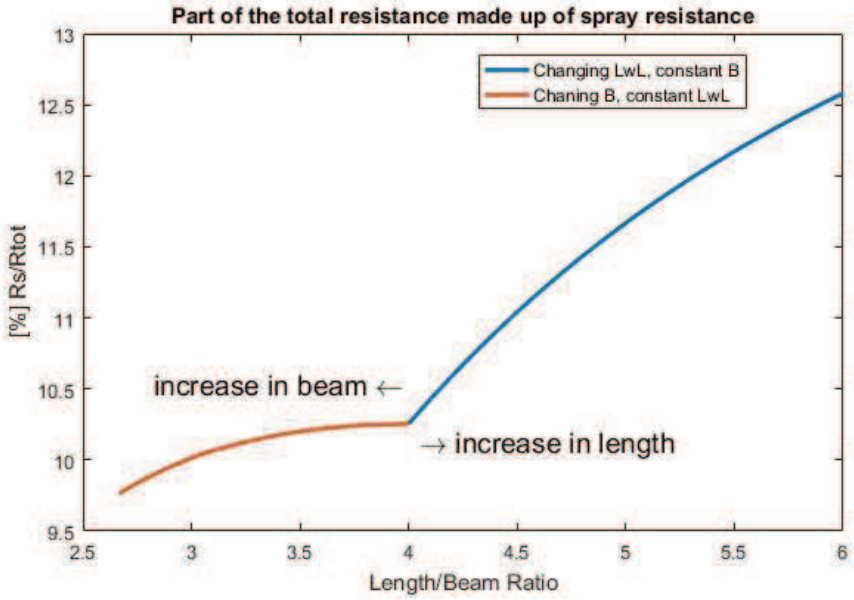

Figure 16. Contribution of spray resistance to total drag as a function of L/B ratio. Initial particulars: $\beta = 20, L = 6\ ft, B = 2\ ft, M = 68.7\ Lbs, V = 25.4\ kt$

The results show that spray resistance becomes a more significant component as the hull gets more slender. It is therefore beneficial to have higher L/B ratios for increasing potential of the spray removing technologies. The results from the Figure 16 will vary depending on scale, deadrise angle, LCG location and speed but are still representative of the general trend.

3.1.7. FINAL DIMENSIONS

The quality of experimental results state improves with increasing model scale since scale increases the magnitude of the forces. In this project, the maximum scale is limited by the constraints listed in Section 3.1.3.

The mass turned out to be the limiting constraint for the scale factor. The mass of the parent hull from Wielgosz (2018) with all the equipment is 14.7 Lb (6.67 kg). Since the maximum model mass was set to be 50 Lb (22.7 kg), the maximum model scale from Froude scaling law (equation (4)) becomes

$$\mu = \sqrt[3]{\frac{50\ Lb}{14.7\ Lb}} \approx 1.5 \tag{42}$$

The remaining linear dimensions were obtained using the scaling factor and the parent hull. The final dimensions are presented in Table 5. The first column shows the dimensions of the parent model and the remaining columns show the final hull dimensions in SI and Imperial units.

Table 5. Final dimensions of the model

Parameter	Parent hull dimensions	Model dimension Imperial units	Model dimensions SI units
Deadrise β	20°	20°	20°
Beam B	$0.24\ m$	$14.2''$	$0.36\ m$
Length overall L_{OA}	$1.22\ m$	$71''$	$1.8\ m$
Waterline length L_{wl}	$1.12\ m$	$66''$	$1.68\ m$
Displacement Δ	$6.67\ kg$	$< 50\ Lb$	$< 22.7\ kg$
L_{wl}/B ratio	4.67	4.67	4.67
LCG	varied	$21.6''$	$0.55\ m$

3.1.8. DESIGN SPEEDS

To check that model satisfies all constraints, Savitsky code was run for the parameters from Table 5. The speed range was tested up to a maximum allowed speed of 36 ft/s (~11 m/s). The resulting prediction of whisker spray forces is shown in Figure 17. To maintain the consistency with the presentation of the results section, the speeds are shown as volumetric Froude number (Fn_∇), which was selected for direct comparison to reference data and to avoid mixing of SI and Imperial units. The displacement was taken from Table 7, Section 3.3.1.

In Figure 17, light-blue bars represent the magnitude of spray resistance using equation (33) and yellow bars show the magnitude of air resistance using equation (34). The blue line going through the spray resistance bars is used to visually show the flow state in the spray area. The slope of the line changes at Fn_∇ 4.7, so starting from Fn_∇ 5.09 the flow in the spray area is assumed to be in the transitional state. The magnitude of the spray exceeds 1 N at Fn_∇ 3.91.

The dark-blue bars show theoretical contribution of spray resistance to total resistance. The requirement of at least 5% contribution is met at Fn_∇ 5.09. It was decided to design one pair of deflectors that would satisfy all the constraints for calm water tests and another pair that would not exceed Fn_∇ 4.3 in wave tests. The selected design speeds are shown in Table 6.

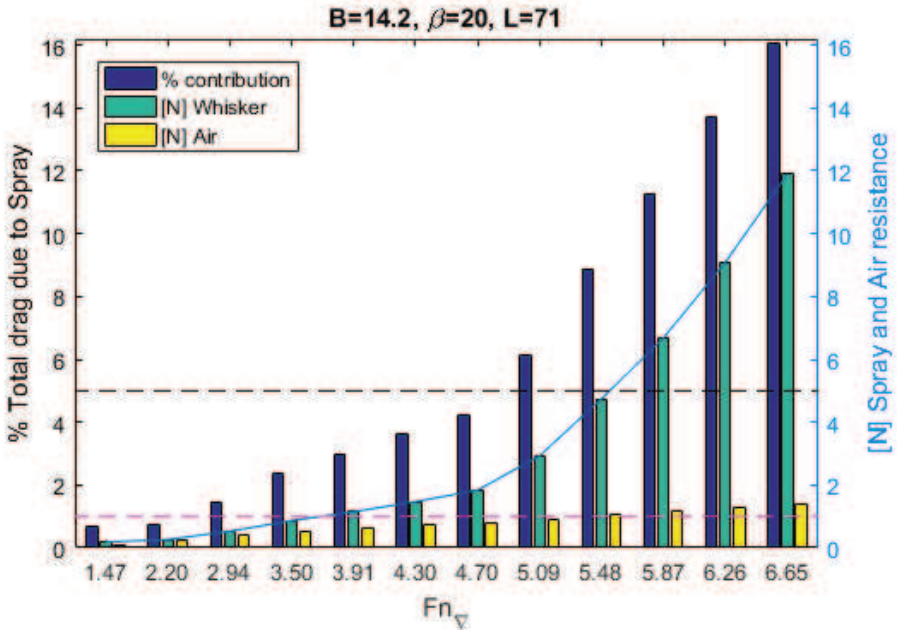

Figure 17. Theoretical magnitude and contribution of spray to total drag for chosen model dimensions

Table 6. Selected design speeds and predicted spray forces

Name & Purpose	Speed Fn_∇	Speed ft/s	Flow state in spray area	Spray magnitude	% of R_{tot}
Deflector 1 (waves)	4.30	23.21	Laminar	1.47 N	3.62 %
Deflector 2 (calm water)	5.87	31.65	Transitional	6.68 N	11.28 %

Each deflector pair is limited to one design speed. The time limitation from production and allocated time for towing tank testing would make it possible to test at most two deflector pairs. The first design speed of Fn_∇ 5.87 was selected to meet the requirements of the spray resistance magnitude, flow state and contribution to total resistance. Fn_∇ 5.87 is above the common operational speeds of HSC (Fn_∇ $1.5 - 4.5$) but is justified for the purpose of spray area testing.

The second speed of Fn_∇ 4.3 does not meet the minimum requirements set for calm water. On the other hand, this speed is more suitable for wave tests as higher speed would mean higher accelerations and put equipment and model at risk. Also, this speed is in the range of typical planing craft operational speeds, so Savitsky Method might be more accurate in predicting resistance components of the hull. This aspect will be investigated in the results section.

3.2. MODEL MANUFACTURING

3.2.1. DESIGN SOFTWARE

The model was designed in Orca 3D®, a plug-in Rhinoceros® – commonly used as a basic hull design tool by practicing Naval Architects. The specific software was selected as it is used in-house for the other projects and to speed up the design process. Orca 3D has a parametric definition of a range of hull shapes including planing craft. This allows to rapidly prototype and visualizes various design parameters.

In this project, major part of the hull length is prismatic except for the bow shape. The parameters given in Table 5 were used to define the outline of the hull shape. The bow was designed to be at least a quarter of the hull's total length. Multiple entrance angles and bow roundness factors were tested to ensure at least 1st order continuity and preferably 2nd order continuity where the prismatic wedge transitions into the bow shape. The list of chosen parameters and more drawings of the model are shown in Appendix B.

3.2.2. INSERT PLATES AND SPRAY RAILS

The sizing of the pocket in the hull was dependent on the maximum expected wetted keel length L_k. The wetted lengths were found using Savitsky code in Matlab. The speeds were varied from Fn_∇ 3 till 6.65 (16.8-35.8 ft/s).

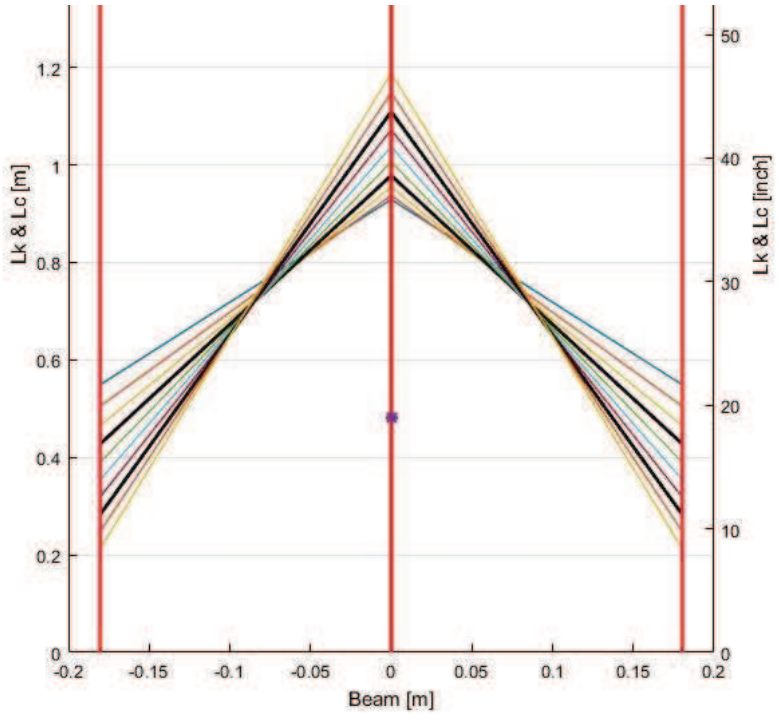

Figure 18. Expected stagnation line locations for the bare hull

The expected stagnation lines were plotted using equation (29). In Figure 18, the view is projected at the hull bottom. Red line at zero beam is the keel line and the other two red lines represent chines. The stagnation lines for the design speeds are represented by the thick black line. In this drawing, the higher speed corresponds to higher L_k and lower L_c, meaning longer stagnation line and a smaller angle with the keel line. The maximum theoretical L_k for this hull is $46.8''$ (1.2 m) at Fn_∇ 6.65.

The pocket length was selected to be $50.4''$ (1.28 m) measured from the stern. The extra allowance was given to ensure space for mechanical attachment of the inserts to the hull bottom and to compensate for any uncertainties in the theoretical model.

For the deflectors, the inserts were designed to run parallel to the stagnation line at a slight offset. Due to workshop and time limitations, the simplest step configuration was chosen – to have constant thickness all the way from keel to chine. This configuration was the only possible solution for a given timeframe and budget at that moment. The chosen design works well if the step is not submerged. A better solution would be to have a tapered step profile that tends to zero thickness as it approaches the keel. The detail drawings for the bare hull and the deflector inserts are shown in Appendix B.

Finally, the spray rails were manufactured according to recommendations from Savitsky et al. (2007, p. 21). The spray area was fitted with three short spray rails per side. This configuration removes approximately 88% of spray area at maximum efficiency and has minimum effect on hull behavior outside of spray area. Locations for spray rails are given in Appendix B.

3.2.3. MANUFACTURING OF THE MODEL

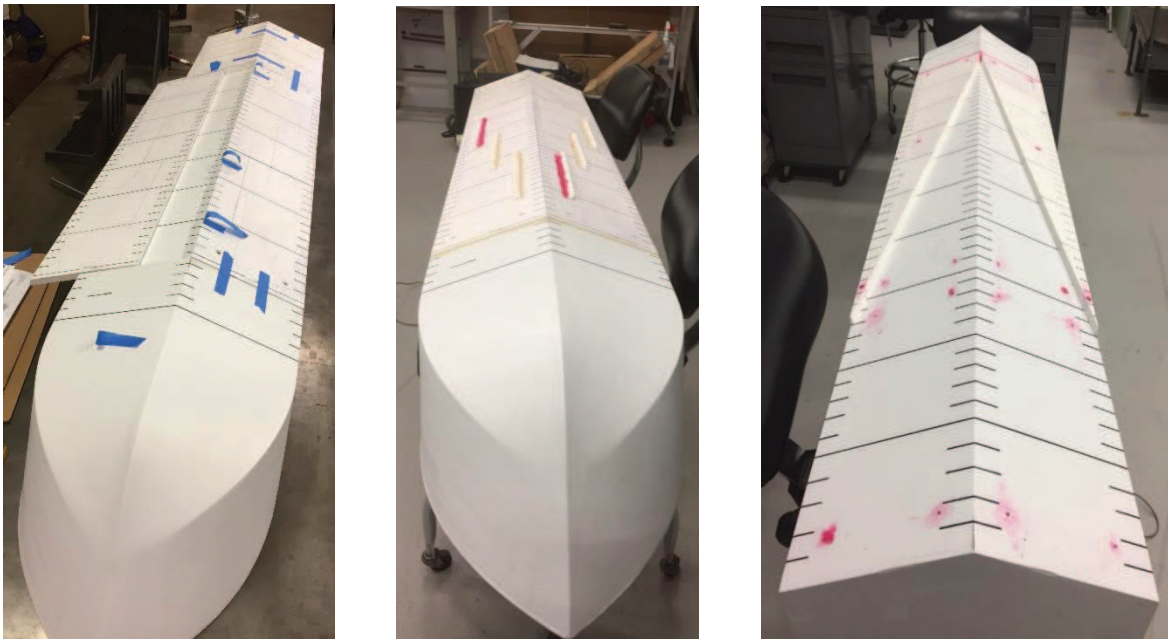

Figure 19. Left to right: Bare hull, Spray rails and Deflectors configurations

The model was milled from a block of FR-7115 closed cell Polyurethane foam using a CNC machine. The surface finish was made by hand using sandpaper. To ensure structural integrity and surface smoothness the cycle of coating model with epoxy resin, drying and polishing were repeated three times. The epoxy used is US Composites 635 in 3:1 ratio with medium speed hardener. Once the smooth surface of reasonable thickness was achieved the model was spray painted with Rust-Oleum® Flat White paint.

The plate inserts were cut out of Expanded PVC Foam. The plates were adjusted to get almost seamless hull bottom. Both the hull and the plates were then marked with $1''$ scale so that wetted keel and chine lengths can be measured from underwater photographs.

Finally, all the seams and screw holes were filled with clay to get a smooth surface finish. The three hull bottom configurations are shown in Figure 19.

3.2.4. INTERNAL STRUCTURE AND EQUIPMENT

The internal structure of the hull, locations and types of installed sensors and equipment is shown in Figure 20 and real experimental set up is shown in Figure 21. The model is restricted in yaw, sway and roll but is free to heave and pitch while surge is controlled by the speed of the towing carriage.

List of equipment

#	Unit Name	LCG Distance from stern [inch]	VCG Distance from keel [inch]	Mass [Lb]
1	Foam hull	31	4.5	21.15
2	Inclinometer+base	12.5	6	0.79
3	Pitch Pivot box+base	21.6	6.25	2.63
4	Drag Balance	21.6	8.75	5.93
5	Attachment bar	21.6	12	1.57
6	Heave Post	21.6	26	5.94
7	CG Accelerometer	17.5	5.95	0.28
8	Bow Accelerometer	51.9	5.95	0.28
9	Aft Ballast	3	7	Varies
10a	CG Ballast	21.6	17	Varies
10b	CG Unload Spring	21.6	-	Varies
11a	Bare Hull Plate	25.6	2.5	7.21
11b	Spray rails	32.5	2.5	0.2
11c	SLR 5.9 Plate	43.5	2.8	2.7
11d	SLR 8 Plate	38.5	2.9	2.97

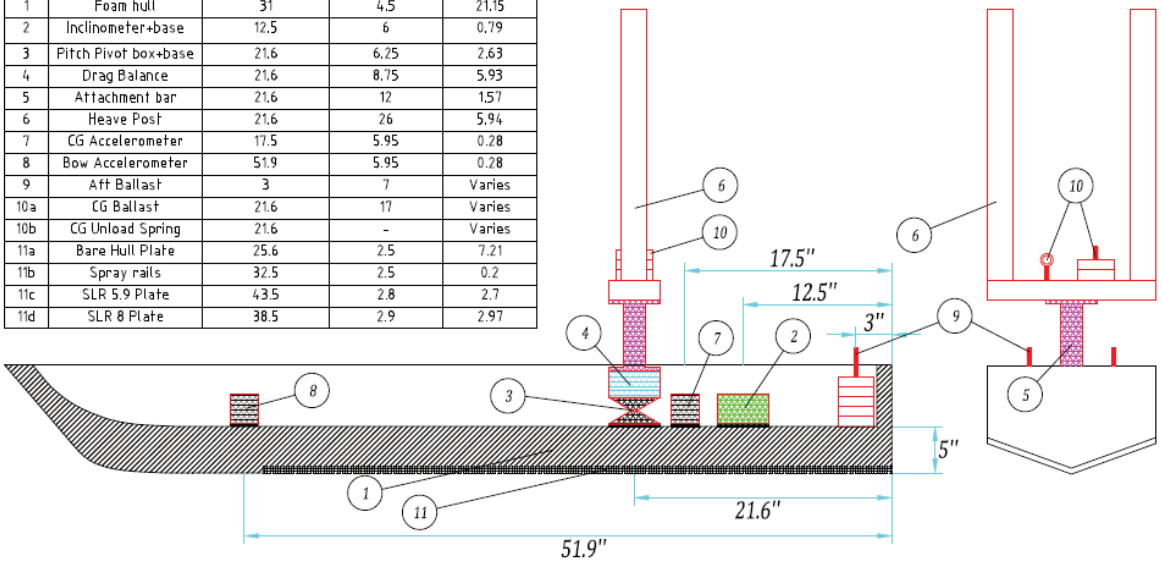

Figure 20. Internal structure and equipment locations

Towing carriage

The carriage (not shown in Figure 20) is an unmanned lightweight structure traveling on a monorail along the towing tank. The towing carriage accommodates two video recording cameras from the starboard and from the stern, data acquisition system and the model itself.

Heave post

The heave post (#6) is a double post attached to the carriage from the top and to the model structure from the bottom. The heave post is locked in all degrees of freedom except for vertical translation. The heave post is a potentiometer, which measures heave relative to chosen zero (static heave). A non-slip thread attached to the heave post and wound around the potentiometer wheel makes it rotate and change output voltage as the heave changes. The calibration is done by changing heave by a known distance and measuring the output voltage. The calibration coefficient is found by fitting a line through the data heave-voltage data.

Accelerometers

The model was fitted with two accelerometers (#7 & 8) to measure accelerations in waves at LCG and at the bow in front of the milled pocket. The accelerometers are closed loop torque-balance transducers attached to the model through base plates screwed into the deck. The accelerometers are calibrated such that at zero trim and at rest the acceleration is measured as 1 g.

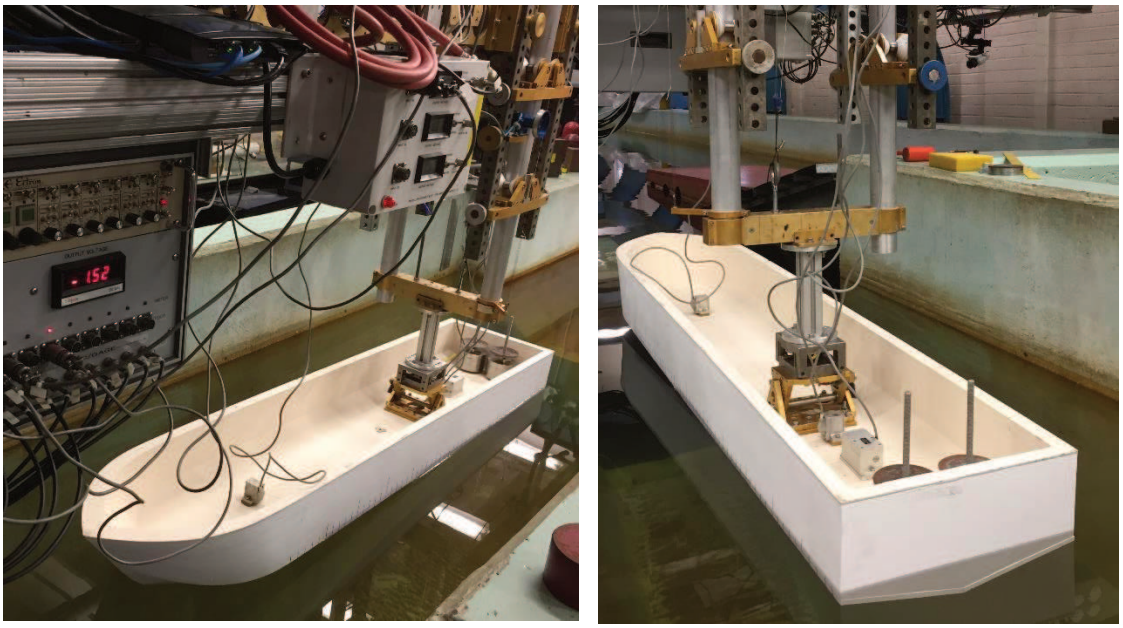

Figure 21. Model attached to the carriage, bow and stern views

Drag Balance

The drag balance (#4) is attached parallel to the deck between the pitch pivot box and heave post. The drag balance is LVDT type (Linear Variable Differential Transducer), which measures shear displacement in thin-walled structure. The displacement is converted to voltage, which is collected by the data acquisition. The calibration coefficient is found by statically applying a known load to the drag balance and recording the output voltage. The slope of the line fitted through the data points is the coefficient used for converting the voltage to drag.

Pitch Pivot Box

The pitch pivot box (#3) is attached to the hull through the baseplate. In this way, the hull is free to pitch relative to the drag balance, which needs to be always horizontal. It is equipped with a rotational potentiometer, which is used to record all the pitch movements of the hull. The pitch is calibrated in a similar way to the drag balance except the weights are used to change the static trim of the hull and output voltage is then correlated to trim measured by the digital inclinometer. Pitch measurements are needed in the wave tests while calm water tests rely more on inclinometer.

Inclinometer

The inclinometer (#2) is attached to the hull through the base plate. The inclinometer works similarly to the pitch pivot box except it is more precise and is used to measure static and dynamic trim angles. The inclinometer comes pre-calibrated and measures trim relative to the flat horizontal surface, so the output value for static and dynamic trim is always the true trim angle of the hull.

Ballast weights Aft

The aft ballast weights (#9) are located as far in the aft as possible. The weights are typically disc-shaped and kept in place by the threaded bar and a nut. The ballast weights are used to change the LCG position of the hull. To match the design LCG, the model is attached to the heave post and locked in the air. The weights are added or removed from the aft until hull achieves zero trim in the air – in this case, the LCG is exactly at the location of heave post ($21.6''$).

Ballast weights and unload at LCG
The weights and unload at LCG (#10a & 10b) are attached at the heave post. The weights are attached in the same way as in the aft. The unload spring is attached in tension to the carriage. The weights at the LCG do not affect the LCG position but are used to adjust the displacement of the hull. Generally, ballast weights are preferred to control displacement but if the hull is too heavy, springs can be used to decrease displacement. The springs have no effect on the outcome of calm water tests but from the experience of the towing tank might have a small effect on the hull's response to waves.

3.3. EXPERIMENTAL SETUP

The experiments were designed to allow a direct comparison of between the different hull configurations. The calm water tests were focusing on comparison of drag and running position and wave tests were designed to compare accelerations at the bow and at the LCG.

The first series of tests would show how closely the bare hull performance matches the prediction of the Savitsky method in the selected speed range. The assumption here is that Savitsky method becomes less accurate with an increase in speed.

Next, the spray rail and deflector hull configuration would be tested for the same speed ranges and the same LCG position. Here it would be possible to see how redirecting flow in the spray area influences the running position of the hull and total resistance.

Finally, if the difference is too high, the LCG position of the bare hull would be adjusted to match the equilibrium running position of the deflector hulls, which would allow to eliminate the pressure area from the analysis and compare only the forces in the spray area.

For the waves, the bare hull was compared against spray rails and deflector designed for the lower speeds (Fn_∇ 4.3). All the tests were performed at the same LCG at pre-planing and fully planing speed.

3.3.1. MODEL PARAMETERS

Table 7. Model parameters for the experimental tests and Savitsky Matlab code

Property	All hulls, Imperial units	All hulls, SI units
Deadrise β	20°	20°
Beam B	$14.2''$	$0.36\ m$
Waterline length L_{wl}	$66''$	$1.68\ m$
Displacement Δ	$46.06\ Lb$	$20.89\ kg$
VCG	$\sim 5.25''$	$\sim 0.13\ m$
f	$\sim 2''$	$\sim 0.05\ m$
LCG 1	$21.6'$	$0.55\ m$
C_{Air}	0.7	0.7

A total of four hull configurations were tested: bare hull, spray rails and two deflector sets. The hulls had different weight distribution due to the varying weight of the plate inserts, but all were adjusted to have design LCG and same weight. The VCG varied slightly but from the towing tank experience, the location of VCG has a negligible impact on hull's trim and drag results. The parameters listed in Table 7 were used both for model tests and for Savitsky code.

3.3.2. CALM WATER TESTS

The test matrices were built around the selected design speeds and test assumptions. The deflector 1 and deflector 2 pairs were designed for design speeds of Fn_∇ 4.3 & 5.87 respectively.

The bare hull and the spray rail hulls were run at twice as large increment than the deflector hulls to allow for direct comparison. In addition, the bare hull speeds were extended to include lower speeds (Fn_∇ 1.47, 2.20 & 2.94) for comparison to the Savitsky Method as a proof of concept.

The calm water test matrix is summarized in Figure 22. The deflectors were tested for speeds Fn_∇ $3.52 - 6.65$ with about 0.4 Fn_∇ increment. Since the deflectors would not be effective too far outside the design speed range, the only point of overlap is the speed at Fn_∇ 5.09. The bare hull and spray rails were tested at larger speed increments aiming to include the most important points for comparison – design speeds, overlap speed as well as the lowest and the highest speeds.

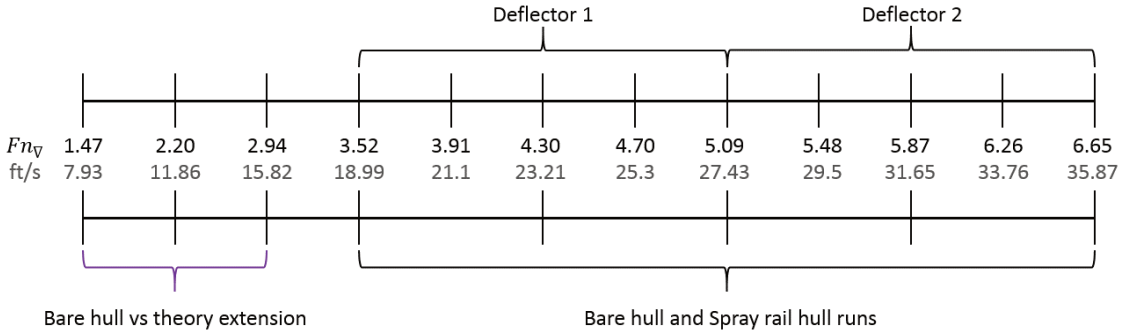

Figure 22. Speeds used for calm water tests for different hull configurations

Each run was done at least twice to ensure repeatability and estimate measurement error. More information about repeatability, error measurement and test matrix planning are given in Lundmark (2018).

Before the tests the model was assembled, weighted and balanced in the air to find correct LCG position. Then, the measurement equipment was zeroed in static floating condition and finally, static trim and heave were measured. Each run would include setting up towing speed, camera settings, running and returning the model. Between runs, the waiting time was about 6 minutes to allow the water in the towing tank to reach calm state for the next run.

For each test run the total drag, heave at LCG, trim and the actual carriage speeds were measured and documented. In addition, underwater and overwater pictures were taken, which allow to see measure wetted area and see flow behavior. The entire run from the start to the end was filmed using video cameras attached to the towing carriage.

3.3.3. IRREGULAR WAVE TESTS

For the irregular wave tests, the sea state 2 was selected and generated with Pierson-Moskowitz spectrum. The significant wave height H_s and wave period T_p were scaled up from Wielgosz (2018) to the model scale using the Froude law of scaling. The test parameters are summarized in Table 8. Due to time limitations, the deflector pair #2 was not tested in waves.

The low speed of SLR 2 (Fn_∇ 1.47) was chosen as a pre-planing speed, for which the hull is expected to follow the wave profile. The SLR 5.86 (Fn_∇ 4.30) is the design speed for deflector #1. At this speed, the hull is expected to skim from peak to peak and experience high accelerations. (Savitsky and Brown, 1976)

Table 8. Testing parameters for the acceleration measurements

H_s	T_p	Pre-planing speed	Planing speed	LCG location
$3.788''$ $0.096\ m$	$1.557\ s$	$SLR\ 2$ $Fn_\nabla\ 1.47$	$SLR\ 5.86$ $Fn_\nabla\ 4.30$	$21.6\ ''$ $0.55\ m$

The preparation for the wave tests was similar to the calm water tests except the underwater camera could not be used in waves. Then, the wavemaker was turned on to generate the sea state. After 2 minutes a fully developed sea state would be reached, and the test was initiated.

Since accelerations are based on wave encounter statistics, the model was towed enough times to reach 100 encounters in both heave and pitch as suggested in ITTC (1999, chap. 2.2.11). To ensure that the model was not towed twice through the same waves, the wave spectrum was offset by a few seconds before each run. The offset was kept the same between the hull configuration to ensure as similar wave encounters as possible.

During the test, the accelerations at the bow and at the LCG were measured along with pitch, heave and encountered wave height. The results were then post-processed in Matlab to get time history graphs and acceleration statistics.

4. RESULTS

4.1. CALM WATER TESTS

The following sections show results for calm water tests. The trim angles are shown in degrees. The forces are normalized by the displacement of the hull $\boldsymbol{R_T/\Delta}$ and heave by the cubic root of hull volume $\boldsymbol{H/\sqrt[3]{\nabla}}$.

First, the comparison is done between the empirical and experimental results of the bare hull. Next, the experimental bare hull results are compared to other hull configurations. The colors assigned to the hull types stay consistent throughout the entire section. The raw data for experiments is given in Appendix C.

4.1.1. BARE HULL EXPERIMENTS

The results from bare hull testing were plotted against the predicted results from Savitsky Matlab code. Figure 23 shows how Savitsky Method overpredicts hull's trim angle by approximately 0.6°.

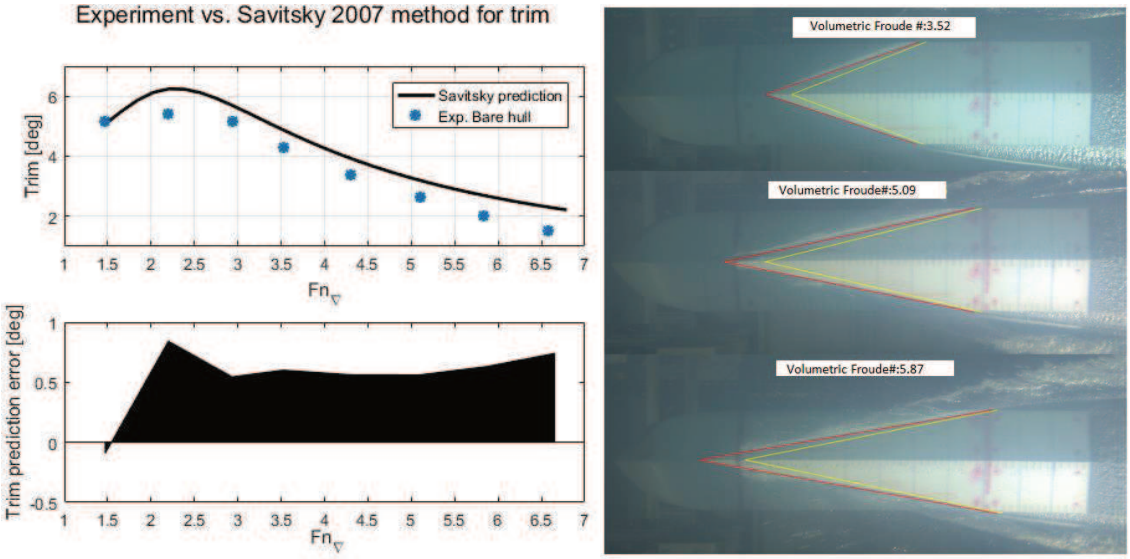

Figure 23. Empirical method vs experiments. Left: trim angles. Right: stagnation line locations

The location of the stagnation line depends directly on the trim angle of the hull. The mismatch between the theoretical stagnation line (yellow) and the experimental line (red) captured by the underwater camera is shown on the right side of Figure 23.

The difference between the measured and predicted resistance is shown in Figure 24. As a final check, the experimental values of the wetted keel and chine lengths, as well as measured trim, were used to estimate total resistance (yellow markers in Figure 24). Both methods were compared against measured resistance and prediction error was plotted in the bar graph in corresponding colors.

The empirical method becomes less accurate with higher speeds, reaching about 15% underprediction at $F_{n\nabla}$ 4.3. The reverse-calculated resistance from experimental results is also inaccurate but gives better resistance estimation at $F_{n\nabla} > 4.3$ for this hull.

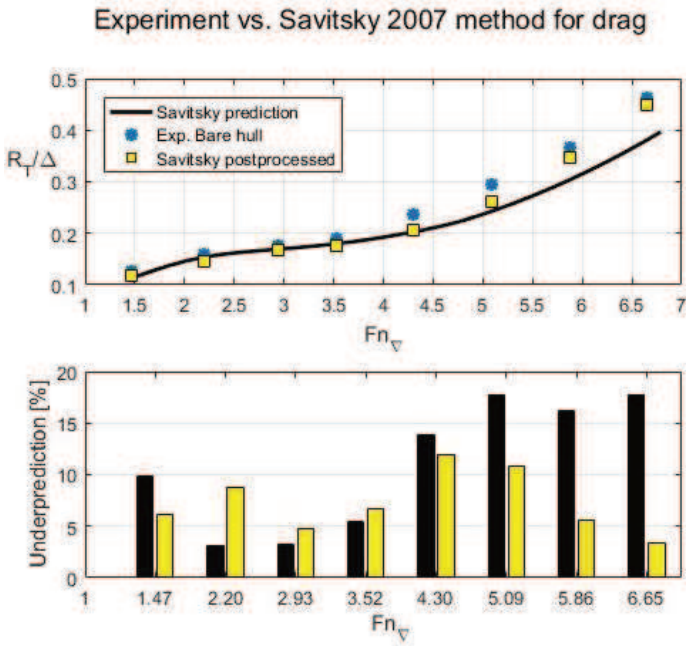

Figure 24. Total resistance comparison. Empirical method vs experiments

4.1.2. SPRAY RAILS EXPERIMENTS

The spray rail configuration did not show significant variation in trim angles when compared to the bare hull (Figure 25). The trim differed by up to 0.1°, which is an acceptable error for direct comparison of the results.

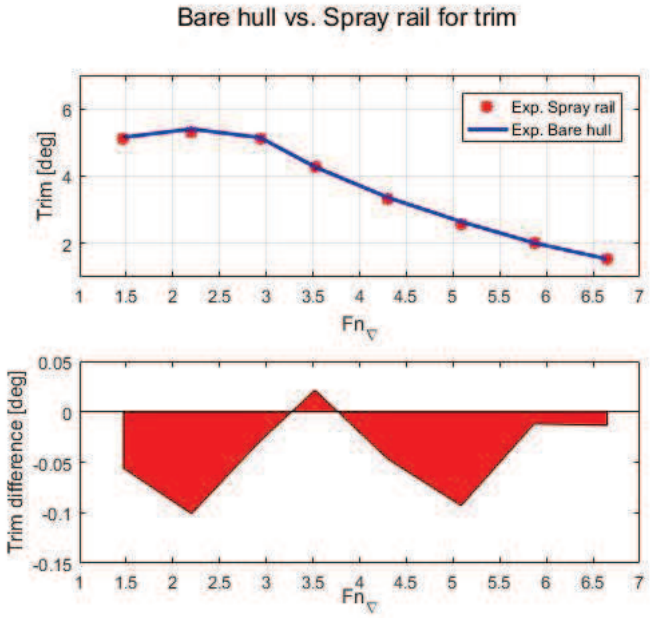

Figure 25. Trim comparison between bare hull and spray rails configuration

The difference in measured resistance is shown in Figure 26. Up until $F_{n\nabla}$ 3.5 the spray rails are submerged and cause an increase in drag but as the hull reaches fully planing speeds, up to 9% in drag reduction is achieved.

A similar situation was observed for heave. Starting from the planing speeds, the spray rails increased heave by up to 7% as compared to bare hull configuration (Figure 27).

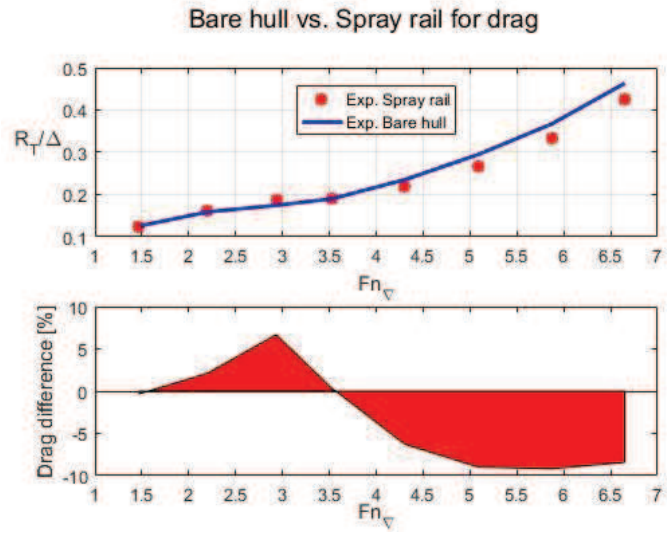

Figure 26. Total resistance comparison between the bare hull and spray rail configuration

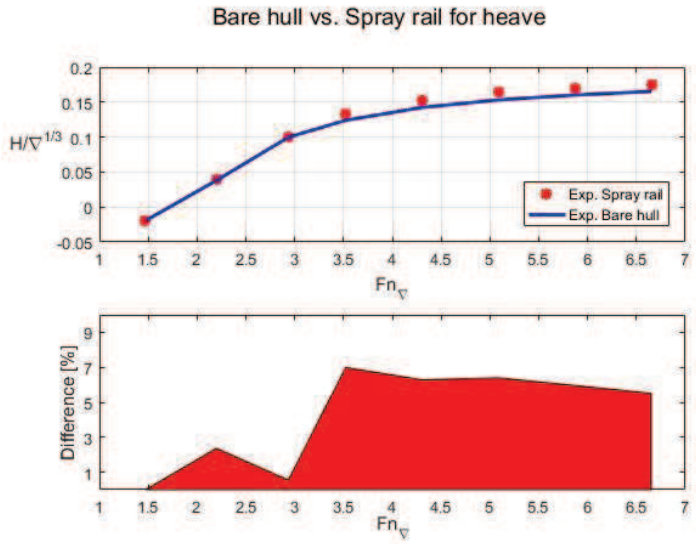

Figure 27. Heave comparison between the bare hull and spray rail configuration

4.1.3. DEFLECTORS EXPERIMENTS

The deflector configurations have significantly changed the running position of the hull. As seen in Figure 28 the deflector hulls attain approximately 1° higher trim angle for all tested speeds. Interestingly, both deflector setups attained almost the same running position at a common speed of $F_{n\nabla}$ 5.09 albeit the difference in static trim between two configurations was higher.

Figure 29 shows running position and spray pattern for all three hull configurations at $F_{n\nabla}$ 4.3. It is visible that spray rail and bare hull (middle and top shots respectively) have lower trim than the deflector hull. A closer look shows the differences in the spray patterns. For bare hull, there is a thin sheet of spray separating from the chine forward of the LCG (heave post). For the spray rails, the spray separation at the chine is approximately at the LCG of the hull and additional spray sheets are created at the spray rails. Finally, for deflector hull, the spray separates behind the LCG. The spray area looks dry and the main spray is more turbulent than in the other two cases.

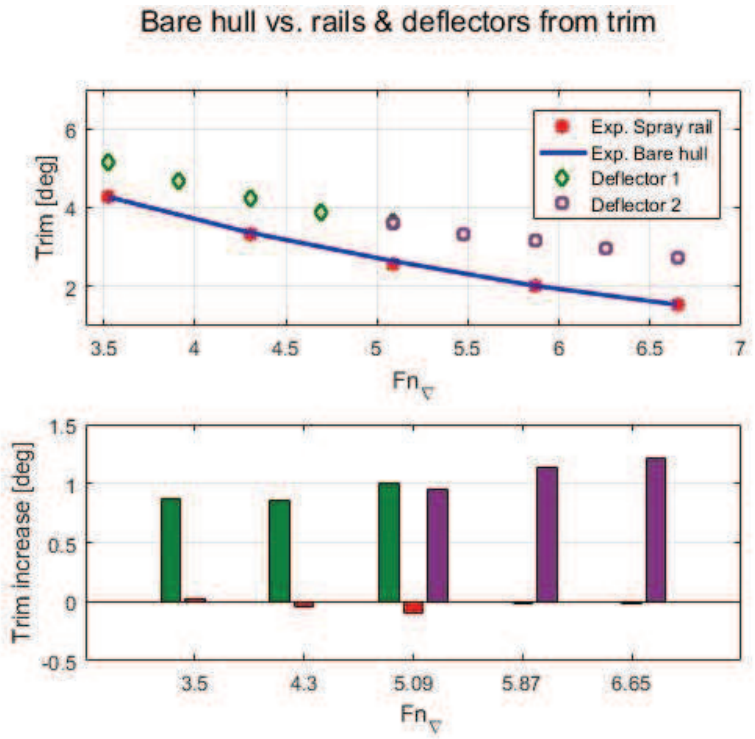

Figure 28. Trim comparison: spray rails and deflector configurations vs bare hull

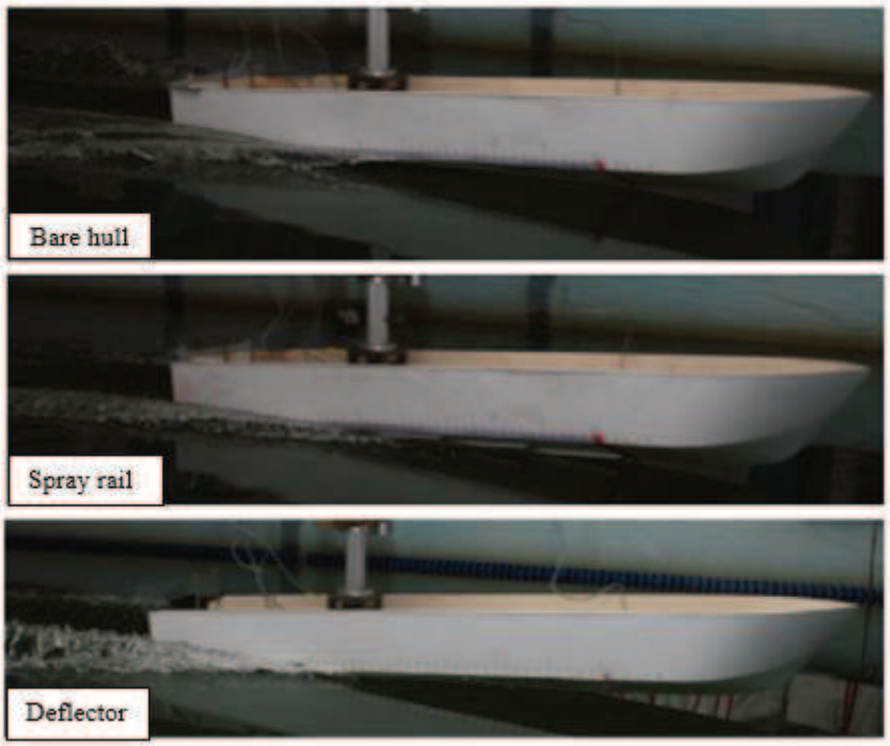

Figure 29. Running positions, same speed. Top to bottom: Bare hull, Spray rails, Deflectors

The total resistance for all configurations was then plotted and compared against bare hull results (Figure 30). Despite higher dynamic trim, the deflector configurations had lower resistance than the bare hull and spray rails configuration.

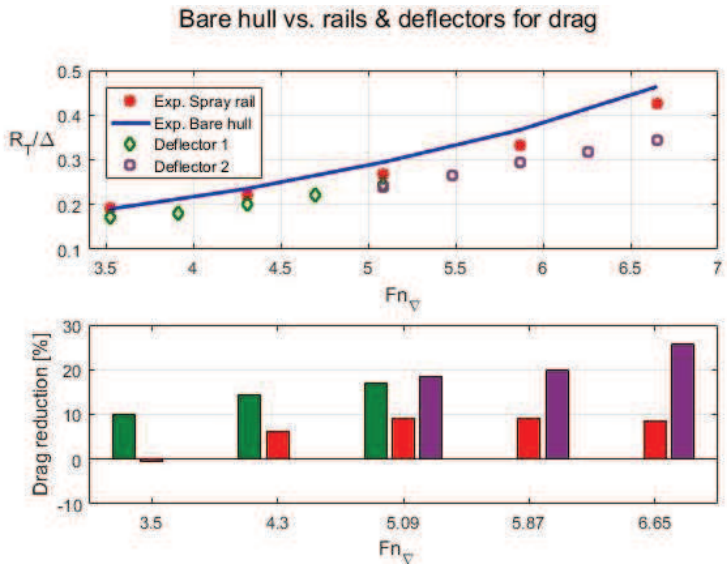

Figure 30. Total resistance comparison against bare hull configuration

The deflectors were twice more effective than the spray rails at the design speeds. It was expected that the deflectors would be effective at the design speed and that the efficiency would drop at lower and higher speeds. Looking at the bottom subplot of Figure 30 the efficiency keeps increasing above the design speeds for both deflector pairs. The maximum achieved drag reduction was at $F_{n\nabla}$ 6.65, where resistance decreased by 25.75% as compared to the bare hull drag.

On the other hand, however, the extra lift gained from the deflector pair seems to decline after the design speed is reached. This can be seen by comparing heave measured for spray rails and the deflector pair #1 (Figure 31). At lower speeds, the heave is similar for spray rails and deflector but after the design speed $F_{n\nabla}$ 4.3, the lift from the deflectors starts to approach same lift as in bare hull configuration.

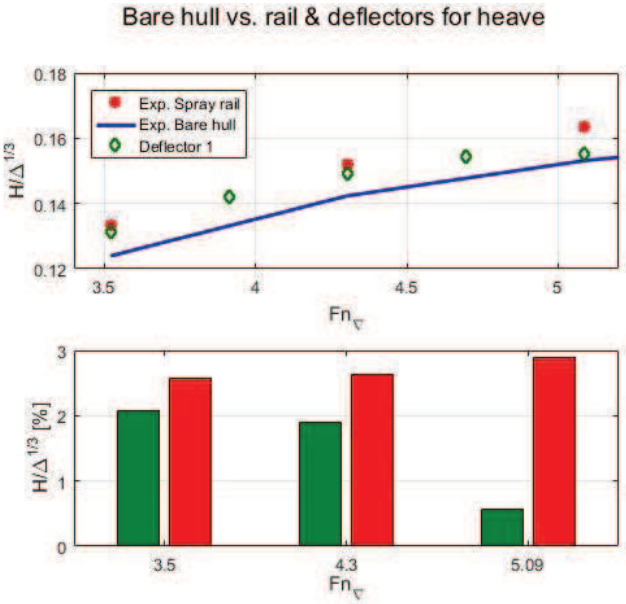

Figure 31. Lift generated by spray rails vs deflector configurations

Figure 32 shows differences in underwater flow behavior for the three hulls at the design speed of $F_{n\nabla}$ 4.3. The wetted keel and chine are the same for the bare hull and the spray

rail set up, meaning that the wetted area is the same. The stagnation line crosses the spray rails, meaning that they are not fully effective at this speed. For the deflector hull, the pressure area is considerably smaller due to the larger trim angle at comparably same heave.

In addition, the wetted area of the deflector hull was further reduced by $0.5''$ rise of keel behind the step. This can be seen from the darker area between the step and the pressure area along the keel – after the keel emerges from the water, the step's edge slightly touches it again. This means that in addition to removing and partially redirecting spray, this deflector design acts as a small step and further reduces resistance by reducing the pressure area of the hull.

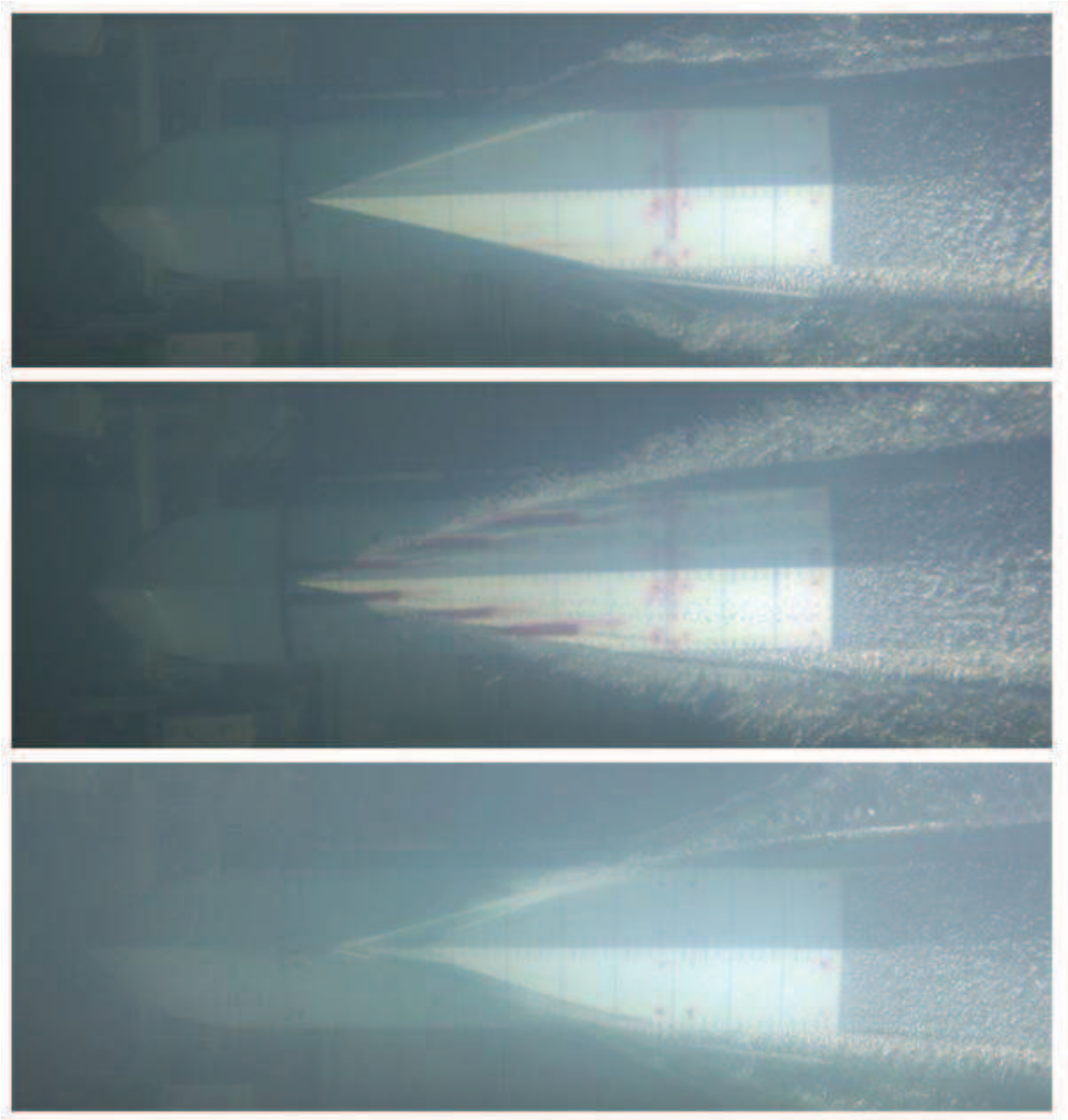

Figure 32. Bottom view $F_{n\nabla}$ 4.3. Top to bottom: Bare hull, Spray rails, Deflectors

4.2. IRREGULAR WAVES TESTS

The snapshots from the wave tests are shown in Figure 33. The bare hull is in the top row, spray rails in the middle and deflectors are shown in the bottom row.

Figure 33. Irregular waves; 1st col.: low speed. 2nd col.: fly over. 3rd col.: bow impact

The columns are organized by the observed effect. The first column is for the displacement speed $F_{n\nabla}$ 1.47. At this speed, all the hull configurations were observed to follow wave profile. The second column shows the fly over phenomenon at high speed, when the entire hull emerges completely from the wave elevation. Finally, the third column shows the bow impact.

Table 9. Acceleration statistics comparison: bare hull and deflector vs. spray rails

Speed	Statistics	Spray Rail [g]	Bare hull [g]	Diff [g]	Deflector [g]	Diff [g]
$F_{n\nabla}$ 1.47	LCG 1/3	0.45	0.37	-0.08	0.52	0.07
	LCG 1/10	0.71	0.56	-0.15	0.90	0.19
	LCG Extreme	1.49	1.09	-0.40	2.58	1.09
	Bow 1/3	1.49	1.48	-0.01	1.30	-0.19
	Bow 1/10	2.58	2.55	-0.03	2.64	0.06
	Bow Extreme	5.02	4.92	-0.10	5.03	0.01
$F_{n\nabla}$ 4.30	LCG 1/3	1.09	1.01	-0.08	1.10	0.01
	LCG 1/10	1.80	1.60	-0.20	1.93	0.13
	LCG Extreme	4.09	3.30	-0.79	6.28	2.19
	Bow 1/3	2.05	2.04	-0.01	1.76	-0.29
	Bow 1/10	3.61	3.64	0.03	3.28	-0.33
	Bow Extreme	7.75	6.88	-0.87	7.83	0.08

The statistics for low and high speeds in waves are presented in Table 9. The spray rails configuration is the baseline against which the deflector and bare hull are compared. Cells colored in green mean that the given hull had lower acceleration statistics than the spray rails setup and vice versa for red colored cells.

The bare hull comparison shows that statistically it has experienced lower accelerations than the spray rail setup. The deflector hull experienced lower accelerations at the bow and slightly worse at the LCG. However, the extreme accelerations at the LCG were significantly higher for deflector hull than for the other two configurations. The statistics from Table 9 are visualized in Figure 34.

Additional information about the tests, run statistics and time histories is provided in Appendix C.

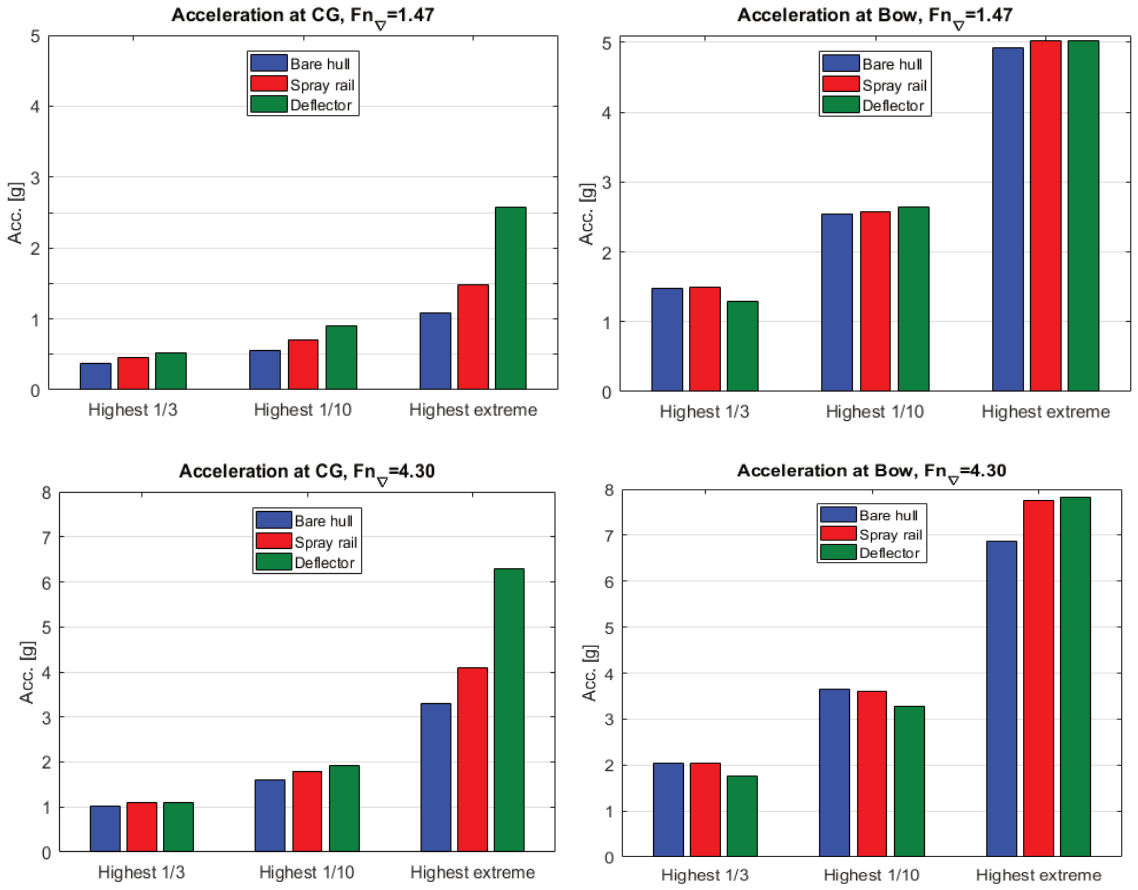

Figure 34. Acceleration statistics for the three hull configurations.

5. DISCUSSION

5.1. RESISTANCE IN CALM WATER

5.1.1. BARE HULL VS EMPIRICAL MODEL

The bare hull design was based on the empirical model. It was shown in results, Figure 23, that predicted trim angles and stagnation lines did not match perfectly with the experimental results. On the other hand, the overprediction of trim is in line with the analysis in Panagiotis (2016, pp. 5–7), showing that empirical methods are helpful for design purposes but are not very accurate even for simple hull shapes.

The results show that Savitsky method yields more than 10% error at pre-planing speeds and at speeds above $F_{n\nabla}$ 4.30. This means that although the Savitsky Method can be used to estimate the proportion of the force components, the error margin makes results inconclusive. Even when experimental trim and pressure area were used, Savitsky Method did not improve much in accuracy. A breakdown of force components for bare hull at speeds $F_{n\nabla}$ 4.30 & 5.86 is shown in Figure 35. In the chart, the total measured resistance is 100%. The forces were reverse-calculated using equation (40) and measured trim, speed and pressure area. Finally, the discrepancy is the difference between the measured and calculated resistance. A breakdown for all speeds is provided in Figure 43 in Appendix C.

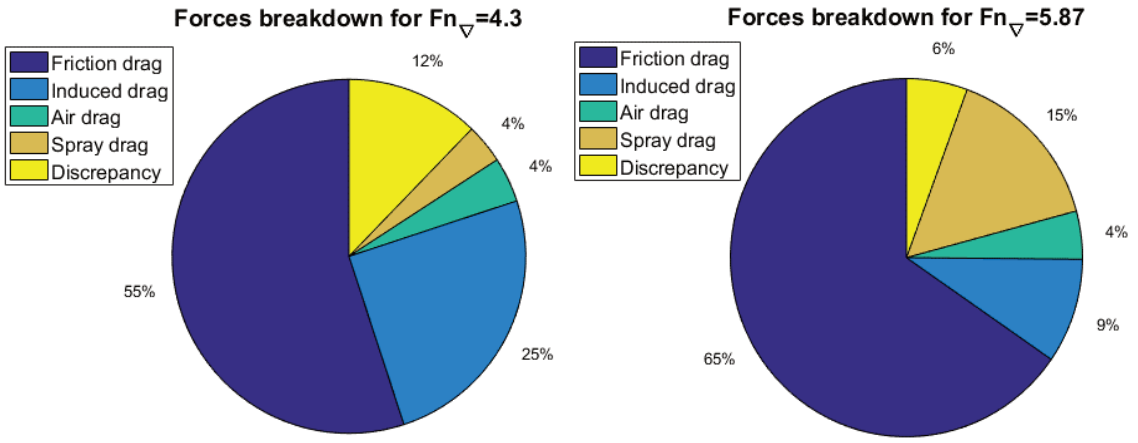

Figure 35. Forces breakdown for bare hull at two design speeds

The discrepancy of 12% and 6% is the same as shown in the bar graph in Figure 24. It is seen from Figure 35 however, that at $F_{n\nabla}$ 4.30 the error is three times larger than predicted spray drag, which means the actual spray drag could differ significantly from calculated. The error between predicted and measured drag also contains the measurement error, which is documented in Table 13, Appendix C. The measurement error accounts for up to 0.6% variance in drag and up to 0.03° in measured trim, which is only a small portion of the discrepancy shown in Figure 35. The other possible sources of the discrepancy between the empirical method and experimental results are discussed below.

The pressure area was calculated from the underwater pictures, which had precision of up to 1 inch and could have been bigger than calculated. The friction forces could have been higher than calculated due to modular design. Although care was taken to make hull as

seamless as possible and all the holes were filled with clay, connection points could have caused an increase in turbulence.

The air and spray drag were calculated using equations (33) and (34), which might not be an accurate assumption for the given model. For example, the flow in the spray area at $F_{n\nabla}$ 4.30 is still laminar but close to transitional according to theory. In an experiment it could have been transitional flow state, which would result in substantially higher spray forces magnitude.

5.1.2. SPRAY RAILS VS BARE HULL

It was observed in results that spray rails did not remove as much spray as they potentially could have in the experiments. To test that assumption, the trim angles measured in the experiments were used in equations (33) and (32) to estimate the magnitude of the spray resistance for the bare hull. In Figure 36 the estimated resistance magnitude is compared to the resistance difference between the bare hull and spray rail configuration. This comparison is fair because the trim angle did not vary between the hulls.

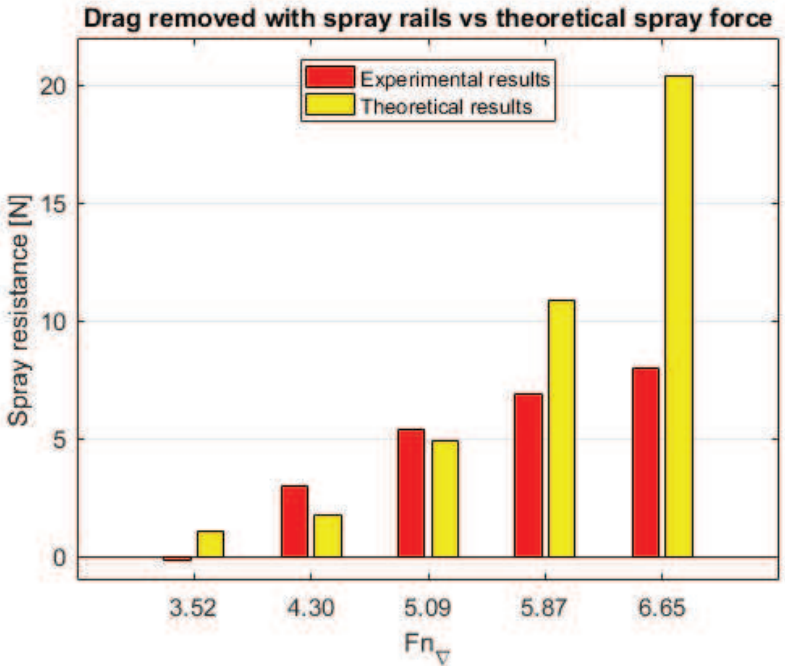

Figure 36. Theoretical spray magnitude vs resistance removed by spray rails

The red bars show the same values as in Figure 26 and yellow bars show theoretical spray resistance. Interestingly, spray rails remove more resistance than the equation (33) predicts for speeds $F_{n\nabla}$ 4.30 & 5.09. This could mean that either theoretical resistance is underpredicted or that spray rails have in addition reduced the pressure area by lifting hull higher of the water.

The underwater pictures of spray rail setup at high speeds showed that spray rails are partially in the spray area and partially in pressure area. This is likely the reason for the drop in efficiency at speeds $F_{n\nabla}$ 5.87 & 6.65 as compared to the theoretical potential.

5.1.3. DEFLECTORS VS BARE HULL & SPRAY RAILS

The trim difference between bare hull and deflector hulls was substantial, which makes it hard to draw definite conclusions about the performance of the deflector technology itself even though the results are promising.

There are several reasons that may have caused a significant change in trim. First of all, the deflector was designed using a theoretical model, which was proven to overpredict trim and therefore underpredict wetted keel and chine lengths. Looking at Figure 32, the perfect deflector would have been placed a few inches forward of the bare hull's stagnation line. Since the deflector was placed behind the real stagnation line, it may have caused the hull to increase trim until the stagnation line matched the deflector geometry.

The reasoning from above is not enough to explain why hull's trim has changed by $\sim 1°$ for all speeds. If deflectors made hull attain the same trim as in the theoretical model, the trim would have increased by approximately $\sim 0.6°$ compared to the bare hull (see Figure 23). The additional $\sim 0.4°$ increase in trim can be attributed to bow up moment created by spray hitting the deflector. Unfortunately, no experiments were done for deflectors at speeds where their efficiency is low, as results may have shown better agreement between the expected and measured trim angles.

As was mentioned previously, the current deflector design reduces pressure area in addition to the spray area. This is caused in part due to increased trim angle and in part due to the geometry of the deflector itself. The typical Petestep deflector design is shown in Figure 37. The thickness of the deflector at the chine is maximum and it tapers down to almost zero as the deflector approaches the keel. The current design has a constant thickness from chine to keel. This feature makes current design a compromise between the Petestep deflector and a step of small thickness.

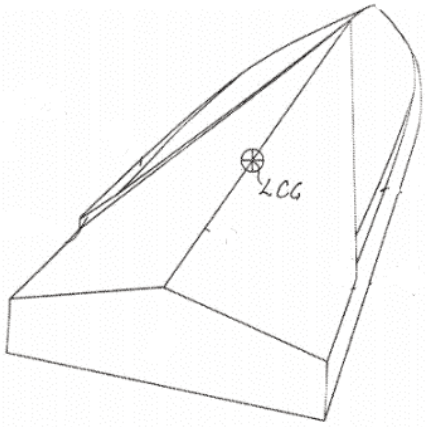

Figure 37. Example PeteStep deflector design (Bjersten and Danielsson, 2014)

The experiments were designed carefully to ensure that deflectors are always forward of the stagnation line so that the thickness difference in hull bottom would not affect pressure area. As seen from Figure 32, this effect was not fully avoided and for some speeds, deflector near the keel line would re-enter water surface due to thickness difference while stagnation line would cross the deflector at its tip near the chine. This could have been avoided with tapered deflector design placed slightly forward of the stagnation line.

Although the deflector design could use some improvement, the deflector hull resistance was the lowest for all tested speeds. At the design speeds the deflector #1 and #2 decreased drag by 15% and 20% respectively compared to the bare hull. It was observed

during experiments and from side-view pictures that the spray area was suppressed by the deflectors. The underwater pictures show more focused wake behind the stern, which indicates that deflectors may have created additional thrust. The magnitudes of the removed spray forces and added thrust could not be calculated due to differences in trim angles and pressure area between the bare and deflector hull.

Finally, experiments were performed in an attempt to match the trim of bare hull to trim of deflector hulls for the design speeds. This was done by moving bare hull LCG aftward until the same running trim was achieved, which would eliminate induced drag and pressure area from the comparison. Unfortunately, the bare hull started porpoising at approximately $4°$ trim at $F_{n\nabla}$ 4.30, which is $0.22°$ lower than trim measured for deflector hull at the same speed. The only conclusion from this experiment was that the deflectors have made the hull more stable longitudinally.

5.2. ACCELERATIONS IN WAVES

The irregular waves experiments have shown that present deflector design experiences about the same accelerations as the spray rails setup. In extreme events, however, deflectors led to significantly higher accelerations at LCG than the other two hulls.

It is likely that the constant thickness of the deflector is not favorable for impact accelerations. Unlike for calm water, submergence of the deflector could not be avoided in waves. As the hull was submerging, the deflector's profile would get in the way of the fluid motion, likely converting its kinetic energy into pressure forces on the hull and therefore increased accelerations.

Finally, the deflector hull experienced higher pitch amplitudes than the other two hulls. This can be seen from Figure 44-Figure 49 and Table 14 in Appendix C. Possibly the tapered deflector design located more forward would cause lower pitch amplitude and decrease the interference of deflector's profile with water during impacts.

6. CONCLUSION

A modular hull with three bottom configurations was developed for the purpose of benchmarking tests for spray deflection technologies. The prediction results of the empirical model were compared to experimental bare hull results. It was found that Savitsky Method overpredicts trim and underpredicts drag, which means it can not be used as an accurate method to theoretically estimate resistance components for the measured total resistance.

The calm water tests carried out at the same LCG have shown a significant reduction in drag for both spray deflection technologies. Spray rails delivered up to 10% in drag reduction and did not affect the running position of the hull. The deflector configurations yielded even higher reduction in drag ranging from 10 to 25% but running trim angle of the deflector setup increased by approximately 1° for all speeds. The spray deflectors have also improved the dynamic stability of the hull.

Therefore, for the current deflector configurations, the significant reduction in total resistance can only be viewed as a combined effect of deflectors redirecting the spray and deflectors causing a change in pressure area and trim angle of the hull. This provides insight into how deflectors affect overall performance, but individual effects cannot be accurately isolated unless the same trim angle is achieved.

With ever-increasing speed requirements, new technologies and approaches are required for meeting the demand and expectations. This work shows a knowledge gap in the phenomenon of spray resistance and highlights an opportunity for significant power requirement reduction at high planing speeds.

The wave tests have shown that current deflectors design does not significantly decrease accelerations when compared to spray rails. Additional experiments are required with improved deflectors placement and geometry for more fair comparison of spray rails and deflector configurations in waves.

7. FUTURE WORK SUGGESTIONS

Although the results of the present work have shown high potential for implementation of the deflector technology, no definite conclusions could be drawn with respect to how much of the spay drag was removed or converted into additional thrust. The following improvements are likely to shed more light on the true potential of the deflector technology.

Deflector's Location
The current deflectors were placed according to the empirical prediction method, which was proven to underpredict location and angle of the stagnation line. A better approach would be to use underwater pictures of the bare hull's stagnation line or more precise prediction methods for correct placement of the deflectors. This improvement is expected to decrease the trim difference between the bare hull and the deflector configurations.

Deflector's Geometry
Further improvement to the design would be to use tapered deflectors as shown in Figure 37. Correctly located and tapered deflector will eliminate the problem of stagnation line crossing deflector near the chine and being too far from deflector at the keel. Since the thickness of the tapered deflector is practically zero at the keel, it will also eliminate problems associated with the tip of the deflector re-entering the water surface as was pointed out in Figure 32. Finally, the reduced cross-section of the deflector is expected to result in lower impact accelerations as compared to the current design.

Speed matrix
It would be useful to see how the deflectors affect hull's running position outside of their efficiency range – being far from stagnation line or even submerged. Possibly, the results would explain better how the deflectors affect hull's trim angle.

Air drag coefficient
The air drag coefficient used in this study was taken from Savitsky et. al (2007) as a suggested coefficient for typical planing hull forms. A better estimation of air drag coefficient would be to do a resistance test of the hull at 0° trim in the air for a few speeds.

Equilibrium trim matching
Most importantly, more tests are required where all three hulls would attain the same trim angle to allow for direct comparison of the results. For the current hull, this might be possible to achieve with tapered deflector design placed forward of the measured stagnation line. Possibly, LCG position of the bare hull would need to be shifted more aft, so care needs to be taken that the same pressure area is achieved.

Flow state in the spray area
The theoretical spray forces and flow state were predicted according to equations shown in Appendix A. The equations are however are based on limited empirical data and need further verification of accuracy.

> *Further analytical and experimental studies of the viscous characteristics of this relatively thin layer of flow are strongly recommended. Of particular usefulness would be experiments that directly measure the whisker spray drag and relate these results to model size. (Savitsky et al., 2007, p. 13)*

8. REFERENCES

Allen, R.G., Jones, R.R., 1972. Prediction of Three-Dimensional Pressure Distributions of V-Shaped Prismatic Wedges during Impact or Planing. Besthesda, MD : Naval Ship Research and Development Center 37.

Bertram, V., 2000. Practical Ship Hydrodynamics. Butterworth-Heinemann.

Bjersten, P., Danielsson, J., 2014. A watercraft vessel with a planing hull. WO2014200407A1.

Clement, E.P., 1964. Reduction of Planing Boat Resistance by Deflection of the Whisker Spray (No. DTMB-1929). David Taylor Model Basin.

De Marco, A., Simone, M., Salvatore, M., Raffaele, S., Luihi, V., 2017. Experimental and numerical hydrodynamic analysis of a stepped planing hull. Applied Ocean Research 64, 135–154. https://doi.org/10.1016/j.apor.2017.02.004

DNV-GL, 2015. Rules for Classification - High Speed and Light Craft, Part 3 Chapter 1.

Eliasson, R., Larsson, L., 2000. Principles of yacht design, 2nd ed. A&C Black, London.

Fridsma, G., 1969. A Systematic Study of Rough-water Performance of Planing Boats (No. 1275). Stevens Institute of Technology, Davidson Laboratory.

ITTC, 2002. 23rd International Towing Tank Conference. Presented at the Specialist Committee on Waves, ITTC, Venice, Italy.

ITTC, 1999. ITTC-Recommended Procedures and Guidelines. High Speed Marine Vehicles Seakeeping Tests.

Kapryan, W.J., Boyd, G.M., 1953. The effect of vertical chine strips on the planing characteristics of V- shaped prismatic surfaces having angles of dead rise of 20 degrees and 40 degrees [WWW Document]. Digital Library. URL https://digital.library.unt.edu/ark:/67531/metadc56762/m1/1/ (accessed 4.9.18).

Kihara, H., 2006. A Computing Method for the Flow Analysis Around a Prismatic Planing-hull, in: HIPER 06: 5th International Conference on High-Performance Marine Vehicles. Australian Maritime College, Launceston, pp. 262–272.

Kim, J., Young Kim, S., You, Y., Rhee, K., Hwan Kim, S., Kim, Y.-G., 2013. Design of high-speed planing hulls for the improvement of resistance and seakeeping performance. International Journal of Naval Architecture and Ocean Engineering 5, 161–177. https://doi.org/10.3744/JNAOE.2013.5.1.161

Kohansal, A., Ghassemi, H., 2010. A numerical modeling of hydrodynamic characteristics of various planing hull forms. Ocean Engineering 37, 498–510. https://doi.org/10.1016/j.oceaneng.2010.01.008

Larsson, L., Raven, H.C., 2010. Ship resistance and flow, Principles of naval architecture Ship resistance and flow. Jersey City, New Jersey.

Latorre, R., 1983. Study of Prismatic Planing Model Spray and Resistance Components. Journal of Ship Research 27, 187–196.

Latorre, R., Ryan, S., 1989. Dimensional and similitude analysis of spray blister sheet from prismatic planing models. Ocean Engineering 16, 71–83. https://doi.org/10.1016/0029-8018(89)90043-7

Lee, J.-G., Jung, K.-H., Suh, S.-B., Chun, H.-H., Lee, I.-W., 2010. A Study on the Hull Form Design of Semi-Planing Round-Bilge Craft. Journal of Ocean Engineering and Technology 24, 59–65.

Locke, F.W.S.J., Bott, H.L., 1943. A Method for Making Qualitative Studies of the Main Spray Characteristics of flying-Boat Hull Models (No. 19930093031). Bureau of Aeronautics, Washington DC.

Lotfi, P., Ashrafizaadeh, M., Esfahan, R.K., 2015. Numerical investigation of a stepped planing hull in calm water. Ocean Engineering Complete, 103–110. https://doi.org/10.1016/j.oceaneng.2014.11.022

Lundmark, S., 2018. Experimental Evaluation of Spray Reduction Technologies (M.Sc, Submitted). KTH Royal Institute of Technology, Stockholm.

McBride, E.E., 1956. An Experimental Investigation of the Scale Relations for the Impinging Water Spray Generated by a Planing Surface (No. NACA-TN-3615). National Aeronautics and Space Administration, Washington DC.

Molland, A.F., Turnock, S.R., Hudson, D.A., 2011. Ship Resistance and Propulsion, in: Ship Resistance and Propulsion: Practical Estimation of Propulsive Power. Cambridge University Press, New York, pp. 12–83. https://doi.org/10.1017/CBO9780511974113

Olin, L., Altimira, M., Danielsson, J., Rosén, A., 2016. Numerical modelling of spray sheet deflection on planing hulls. Proceedings of the IMechE 231, 811–817. https://doi.org/10.1177/1475090216682838

Panagiotis, A., 2016. Planing Hull Resistance Calculation The CAHI Method (Presentation). SNAME Greek Section Meeting, Hoboken, New Jersey.

Parkinson, J.B., 1935. Tank Tests of Model 11-G Flying-boat Hull (No. NACA-TN-531). Langley Aeronautical Lab.

Payne, P.R., 1982. The spray volume shed by an uncambered planing hull in steady planing. Ocean Engineering 9, 373–384. https://doi.org/10.1016/0029-8018(82)90030-0

Petestep AB, 2016. HOC 33P Explorer [WWW Document]. Petestep. URL http://petestep.com/hoc-33p-explorer/ (accessed 6.27.18).

Pierson, J.D., 1950. The Penetration of a Fluid Surface by a Wedge (No. 381). Davidson Towing Tank Laboratory.

Razola, M., Rosén, A., Garme, K., 2014. Allen and Jones revisited. Ocean Engineering 89, 119–133. https://doi.org/10.1016/j.oceaneng.2014.07.005

Rosén, A., 2004. Loads and Responses for Planing Craft in Waves (PhD Thesis). KTH, Stockholm.

Sambraus, A., 1938. Planing-Surface Tests at Large Froude Numbers-Airfoil Comparison. NACA TM 848.

Savitsky, D., 1964. Hydrodynamic design of planing hulls. Marine technology 1, 71–95.

Savitsky, D., Breslin, J.P., 1958. On the Main Spray Generated by Planing Surfaces (No. 678). Davidson Towing Tank Laboratory, Hoboken, New Jersey.

Savitsky, D., Brown, P.W., 1976. Procedures for hydrodynamic evaluation of planing hulls in smooth and rough water. Marine Technology 13, 381–400.

Savitsky, D., DeLorme, M.F., Datla, R., 2007. Inclusion of whisker spray drag in performance prediction method for high-speed planing hulls. Marine Technology 44, 35–56.

Savitsky, D., Morabito, M., 2011. Origin and Characteristics of the Spray Patterns Generated by Planing Hulls. Journal of ship production and Design 27, 63–83.

Seo, J., Choi, H.-K., Jeong, U.-C., 2016. Model tests on resistance and seakeeping performance of wave-piercing high-speed vessel with spray rails. International Journal of Naval Architecture and Ocean Engineering 8, 442–455. https://doi.org/10.1016/j.ijnaoe.2016.05.010

Shoemaker, J.M., 1934. Tank tests of flat and v-bottom planning surfaces. NACA TN 509.

Sottorf, W., 1934. Experiments with planing surfaces. NACA TM 661.

Swedeship AB, 2018. 12 m High Speed Rescue Craft [WWW Document]. URL http://www.swedeship.se/?portfolio=12-m-rescue-vessel (accessed 8.19.18).

Wagner, H., 1932. The phenomenon of impact and planning on water. NACA Translation 1366, National Advisory Committee for Aeronautics, Washington, DC. ZAMM.

Wielgosz, C., 2018. Experimental Evaluation of Novel Spray Deflectors for Planing Hulls (Master's thesis). KTH Royal Institute of Technology, Stockholm.

Wielgosz, C., Fürth, M., Datla, R., Chung, U., 2018. Experimental validation of numerical drag prediction of novel spray deflector design. Presented at the 13th International Marine Design Conference, Helsinki, Finland.

9. APPENDIX A – SPRAY RESISTANCE

This section gives more thorough background for spray resistance calculation and investigates how to maximize the magnitude of resistance. Equations 43-48 are taken from Savitsky et al. (2007).

According to (32), the nondimensional wetted area increase $\Delta\lambda$ is plotted in Figure 38.

$$\Delta\lambda = \frac{Cos\theta}{4\,Sin\theta \times Cos^2\beta}$$

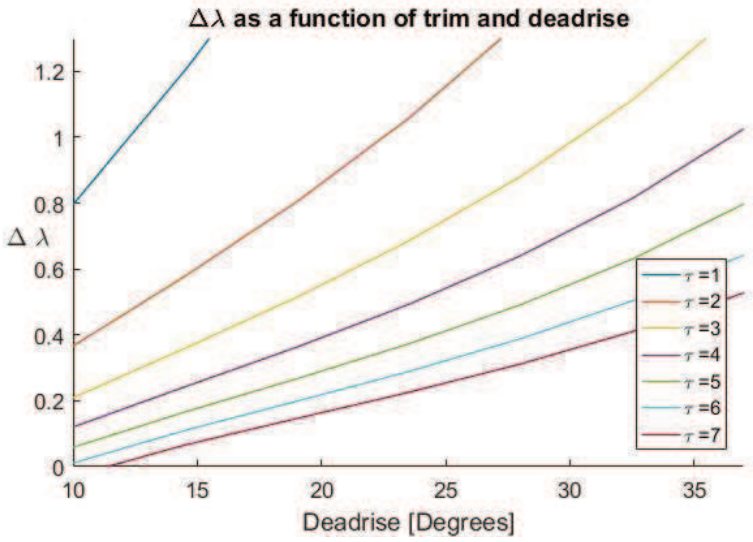

Figure 38. The dependency of wetted spray area on trim and deadrise of the hull

The total force in the spray area is given as

$$F_S = \frac{1}{2}\rho V^2 \frac{B^2}{4\,Sin\theta \times Cos\beta} C_S \tag{43}$$

F_S is defined in the plane of the hull bottom, so it has transversal and vertical components present due to trim and deadrise angle, which do not contribute to the resistance of the hull. To get resistance component in the plane of water surface the correction is made as

$$R_S = F_S \times Cos(\frac{\theta}{Cos\beta}) \times Cos\tau \tag{44}$$

Which, assuming trim angle is small and negligible yields equation (33):

$$R_S = \frac{1}{2}\rho V^2 \frac{B^2 Cos\theta}{4\,Sin\theta \times Cos^2\beta} C_S = \frac{1}{2}\rho V^2\, \Delta\lambda b^2 C_S$$

Savitsky et al (2007, pp. 9–13) highlight that local friction coefficient in whisker spray area C_S in model scale can be laminar, transitional or turbulent while in full scale it is generally turbulent. Therefore, to get more accurate scaling of viscous forces in the spray area it is desirable to at least reach transitional flow. This could be achieved by increasing speed, deadrise or dimensions of the model. The estimate of local friction coefficient C_S are found using the procedure suggested in Savitsky et al. (2007).

The Reynolds number in the spray area is found as

$$R_{eS} = \frac{VL_{WS}}{\nu} \tag{45}$$

L_{WS} is the characteristic length of whisker spray in the spray area, which is found as half-length of the forward edge of the spray sheet. It is smaller than L_m, leading to smaller Reynolds number in the spray area (see Figure 39).

$$L_{WS} = \frac{1}{2} \times \frac{B/2}{Sin\theta \times Cos\beta} \tag{46}$$

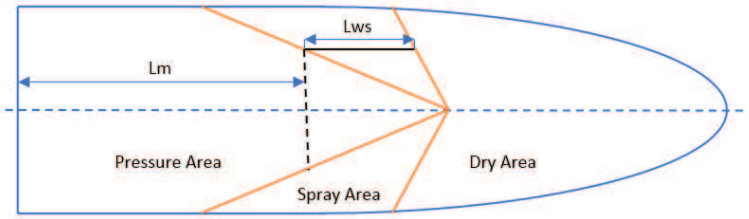

Figure 39. Characteristic spray length L_{WS} and mean wetted length Lm

If $R_{eS} < 1.5 \times 10^6$, flow is expected to be laminar in the spray area and the skin friction coefficient becomes

$$C_S = \frac{1.328}{\sqrt{R_{eS}}} \tag{47}$$

If $R_{eS} > 1.5 \times 10^6$, flow is in a transitional state, having both laminar and turbulent regions present

$$C_S = \frac{0.074}{\sqrt[5]{R_{eS}}} - \frac{4800}{R_{eS}} \tag{48}$$

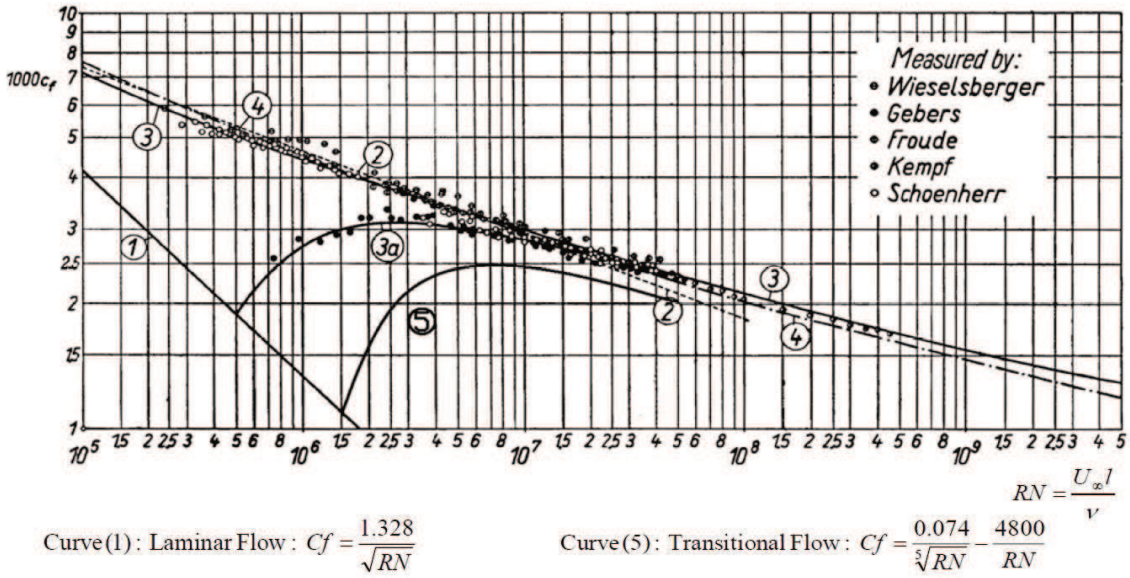

Figure 40. Estimation of C_S as shown in Savitsky et al. (2007, pp. 9–13)

This situation is specific for model scale tests as in full scale flow is typically turbulent. Both equations for laminar and transitional flow are shown in Figure 40 as 1st and 5th curves respectively.

In this section, the attempt is to investigate the dependence of the spray resistance on model's dimensions, trim and speed. Model dimensions from (Wielgosz, 2018) were taken as the basis for investigation (see Table 10). For all the tests SLR of 4 and 6 was checked along with a range of trim angles between 1-7°. In the first series, model dimensions were unchanged. In the later series effect of changing beam, deadrise and scale were investigated separately.

Table 10. Particulars of initial model and studied parameters

Variable	Original model	Studied range
Length between perpendiculars (L_{pp})	1.12 m	1.12-2.4 m
Beam between chines (B)	0.24 m	0.24-0.5 m
Deadrise angle (β)	20°	10-36°
Trim angles (τ)	-	1-7°
Speed to length ratios (SLR)	4-6 $\frac{knot}{\sqrt{ft}}$	4-6 $\frac{knot}{\sqrt{ft}}$

#1 Influence of speed on the friction coefficient

For 1 and 2-degree trim angles, there is a noticeable rapid increase in skin friction coefficient after SLR 4 and 5 respectively. This means that for higher trim angles the spray area is in a fully laminar state.

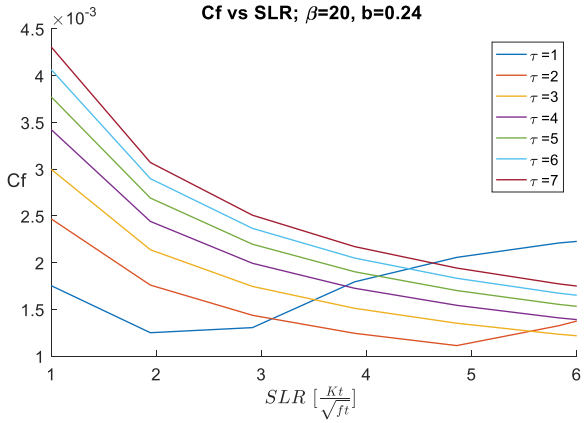

#2 Influence of the deadrise

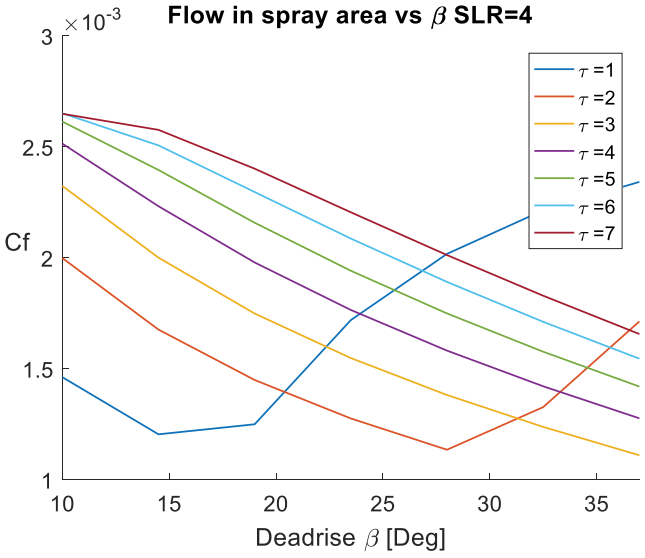

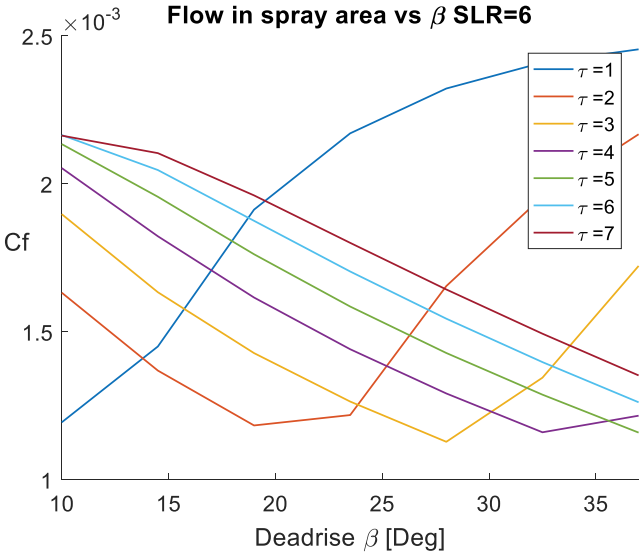

#3 Influence of beam on skin friction

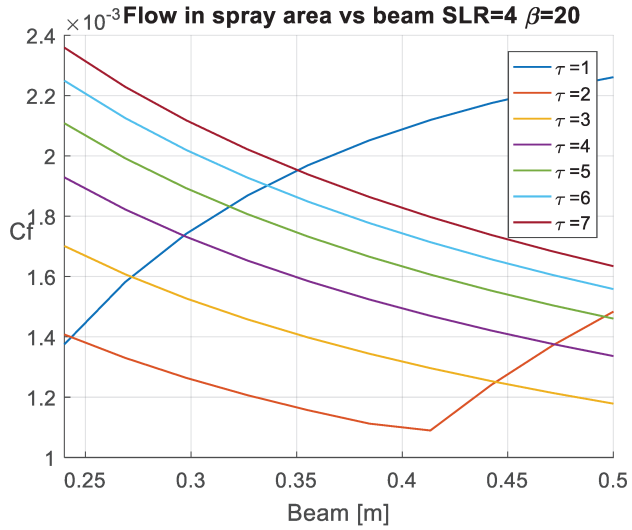

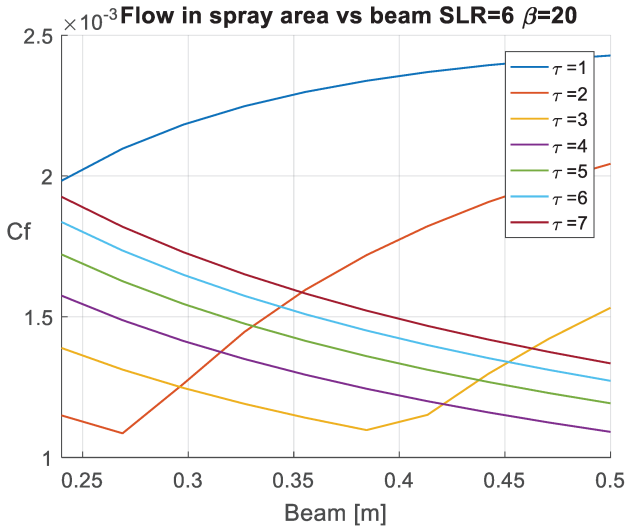

#4 Influence of scale on skin friction

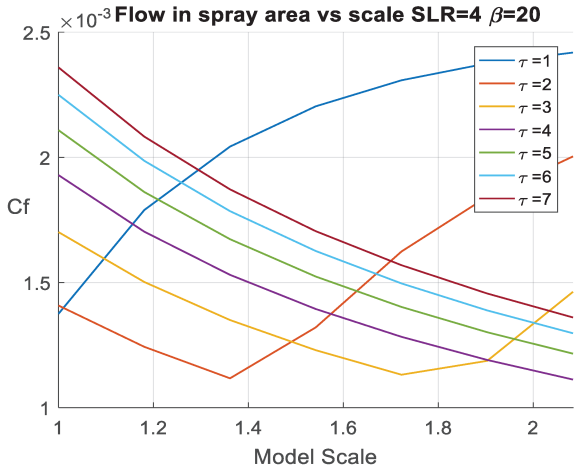

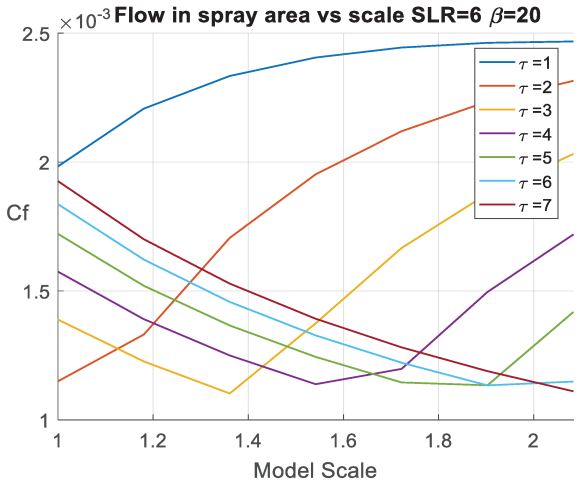

Finally, the original model from Wielgosz (2018) was analyzed for a constant speed of SLR 6 and trim angle of 3 degrees. All of the dimensions were increased by 50% one after the another to show the influence of changes on the spray resistance. The results are shown in Table 11.

The “T” and “L” stand for transitional and laminar flow respectively. Although results are theoretical and can only be used as a guidance, they show the importance of model size for achieving high spray resistance. It is evident that the change in beam has the largest effect on the magnitude of the spray resistance. In addition, once the spray area is in the transitional state, changes in the hull geometry have a higher effect on the spray magnitude than when the spray area is in a laminar state.

Table 11. Effects of hull dimensions on spray resistance

	Test cases ($SLR = 6, \tau = 3°$);					
Parameter	Original	Length	Deadrise	Beam	Scale	All
$L_{wl}\ [m]$	1.12	1.83	1.12	1.12	1.83	1.83
$B\ [m]$	0.24	0.24	0.24	0.36	0.36	0.36
$\beta°$	20	20	30	20	20	30
$flow\ state$	L	L	L	T	T	T
$R_s\ [N]$	0.84	1.14	1.16	1.54	2.63	7.44
Improvement vs original	-	35.5%	38.4%	83.7%	214%	786%
Improvement vs previous	-	35.5%	1.8%	32.8%	70.8%	183%

10. APPENDIX B – MODEL DESIGN

This section gives more details of the hull design. Table 12 gives all the parameters required to reproduce the bare hull surface. Figure 41 shows lines plan of the hull with a pocket used for the plate inserts while Figure 42 shows the hull surface with dimensions in inches.

The CNC drawings along with internal structure were done by workshop engineer and are available upon request.

Table 12. Design parameters of the Hull in Orca 3D

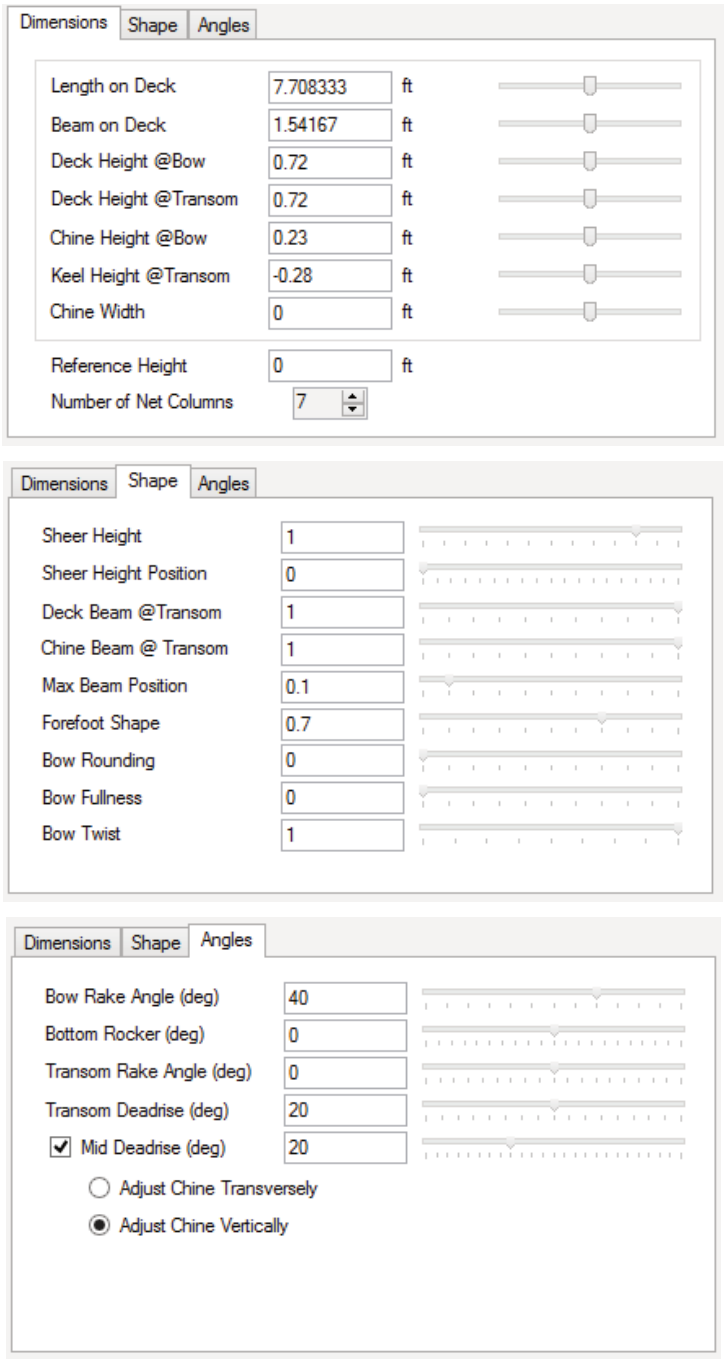

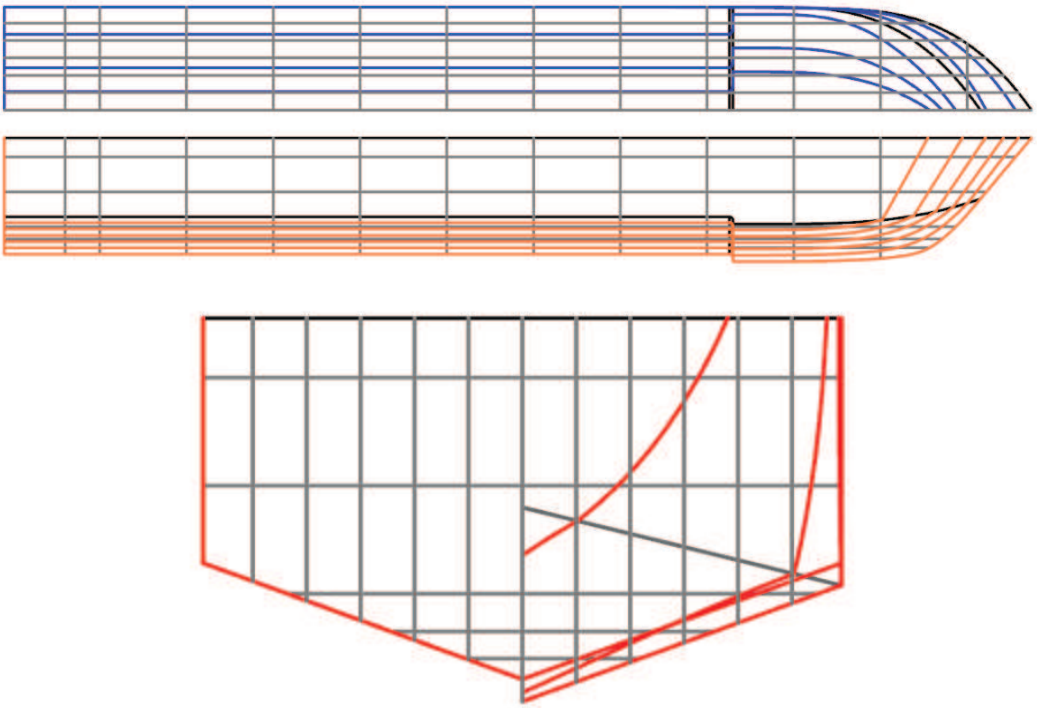

Figure 41. Hull Waterlines (blue), buttocks (orange) and stations (red)

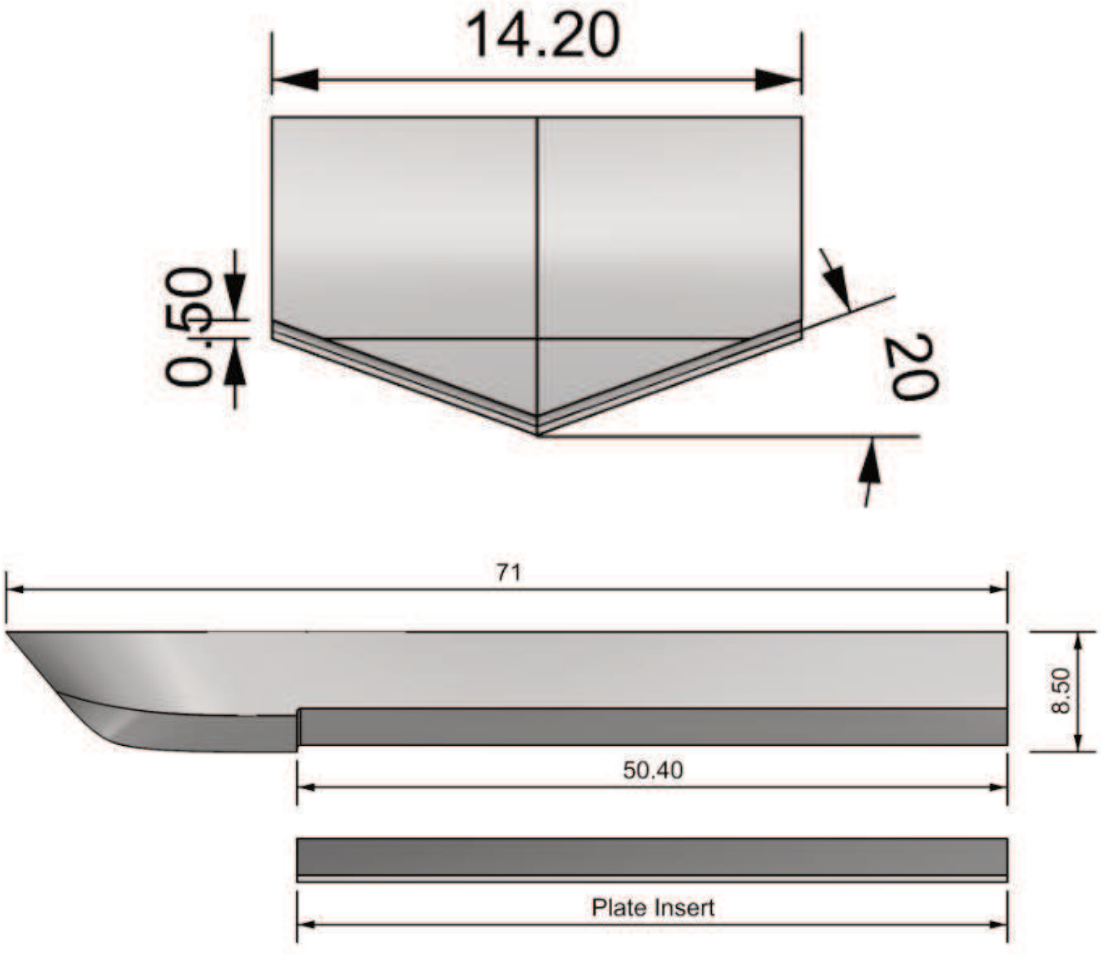

Figure 42. Hull surface with dimensions in inches

Shown below are the PVC plate insert drawings for the bare hull and deflector hull configurations as well as schematic locations of the spray rails (all dimensions in inches).

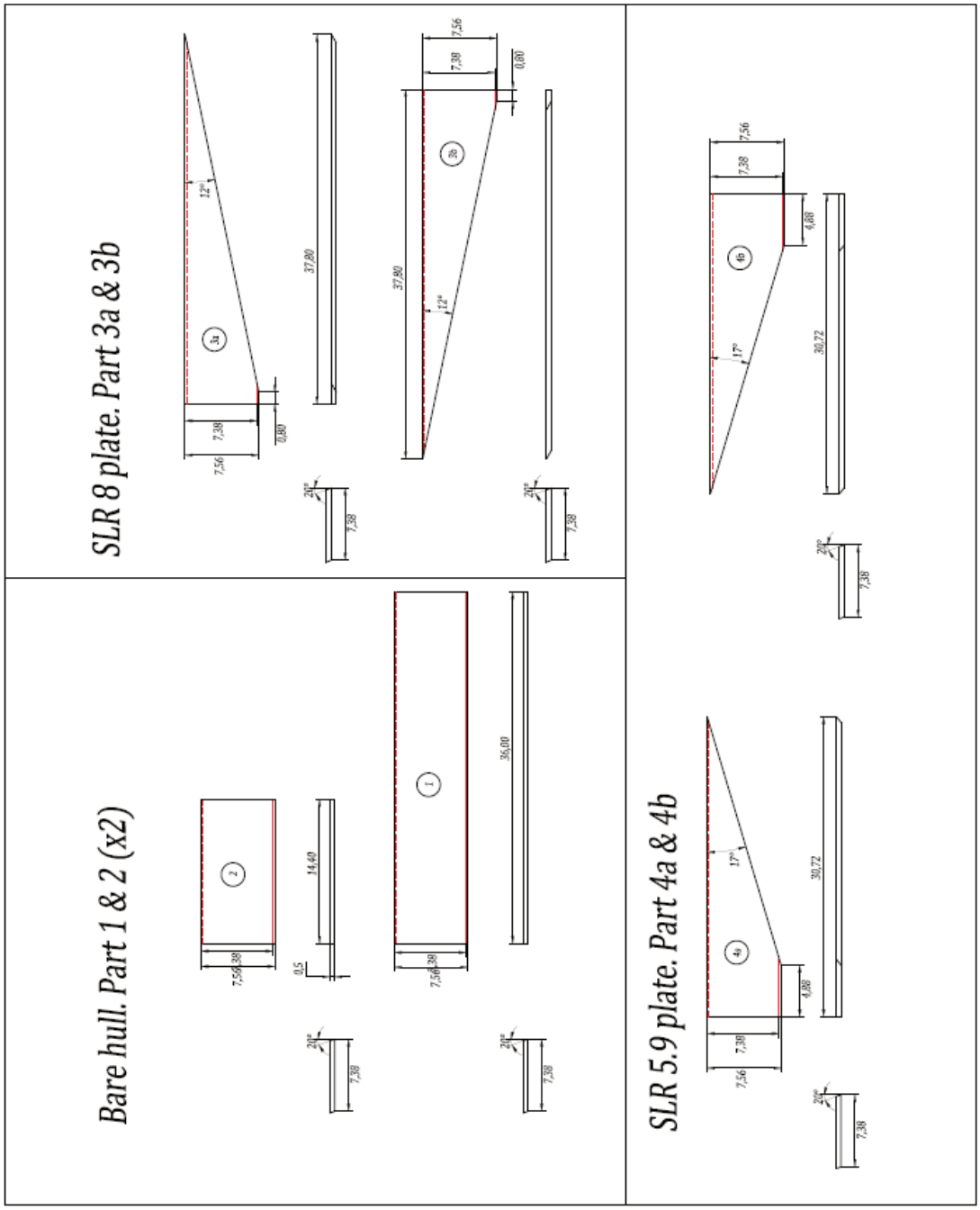

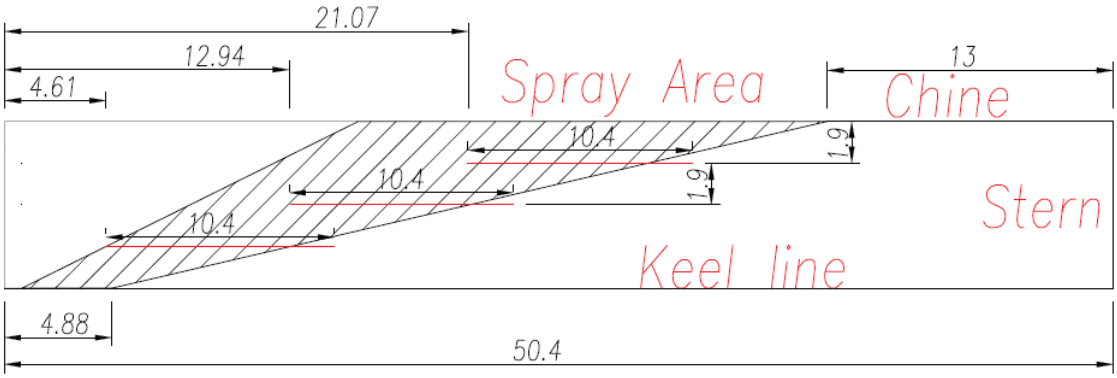

11. APPENDIX C – EXPERIMENTAL DATA

Calm water experimental data

The results for the calm water tests at the same LCG are provided in Table 13. The results shown are averages of multiple runs done at the same speed along with calculated standard deviations for the results. The resistance forces breakdown for bare hull using experimental data and theory from the Savitsky Method is shown in Figure 43.

Table 13. Averaged results and uncertainties for calm water runs

Bare hull average results with standard deviations						
Speed [Fn_∇]	Heave [mm]	u [mm]	Trim [deg]	u [deg]	Drag [N]	u [N]
3.5215	34.1380	0.1016	4.2745	0.0105	38.9040	0.0689
4.3041	39.2050	0.1145	3.365	0.0110	48.2050	0.1579
5.0866	42.1770	0.1143	2.6455	0.0335	60.395	0.0845
5.8692	44.0820	0.0127	2.0160	0.0250	75.2130	0.0645
6.6517	45.5430	0.0127	1.534	0.0080	94.976	0.0111
Spray rails hull average results with standard deviations						
Speed [Fn_∇]	Heave [mm]	u [mm]	Trim [deg]	u [deg]	Drag [N]	u [N]
3.5215	36.7030	-	4.2960	-	39.0580	-
4.3041	41.8340	-	3.3180	-	45.1780	-
5.0866	45.0600	0.0762	2.5525	0.0025	54.9710	0.0467
5.8692	46.8760	0.0635	2.0040	0.0150	68.3080	0.0133
6.6517	48.1840	0.0762	1.5205	0.0035	86.9740	0.1134
Deflector #1 hull average results with standard deviations						
Speed [Fn_∇]	Heave [mm]	u [mm]	Trim [deg]	u [deg]	Drag [N]	u [N]
3.5215	36.2210	0.1524	5.1415	0.0125	34.9610	0.2091
3.9128	39.1420	0.0762	4.6660	0.0110	37.2340	0.1023
4.3041	41.0980	0.2032	4.2210	0.0160	41.2730	0.0534
4.6954	42.4820	0.0635	3.8990	0.0060	45.5590	0.0334
5.0866	42.7490	0.0762	3.6485	0.0015	50.2050	0.0045
Deflector #2 hull average results with standard deviations						
Speed [Fn_∇]	Heave [mm]	u [mm]	Trim [deg]	u [deg]	Drag [N]	u [N]
5.0866	39.6500	0.8766	5.1415	0.0125	34.9610	0.2091
5.4779	40.1070	0.8076	4.6660	0.0110	37.2340	0.1023
5.8692	40.5730	0.6426	4.2210	0.0160	41.2730	0.0534
6.2608	39.7010	0.9059	3.8990	0.0060	45.5590	0.0334
6.6517	41.0470	0.4320	3.6485	0.0015	50.2050	0.0045

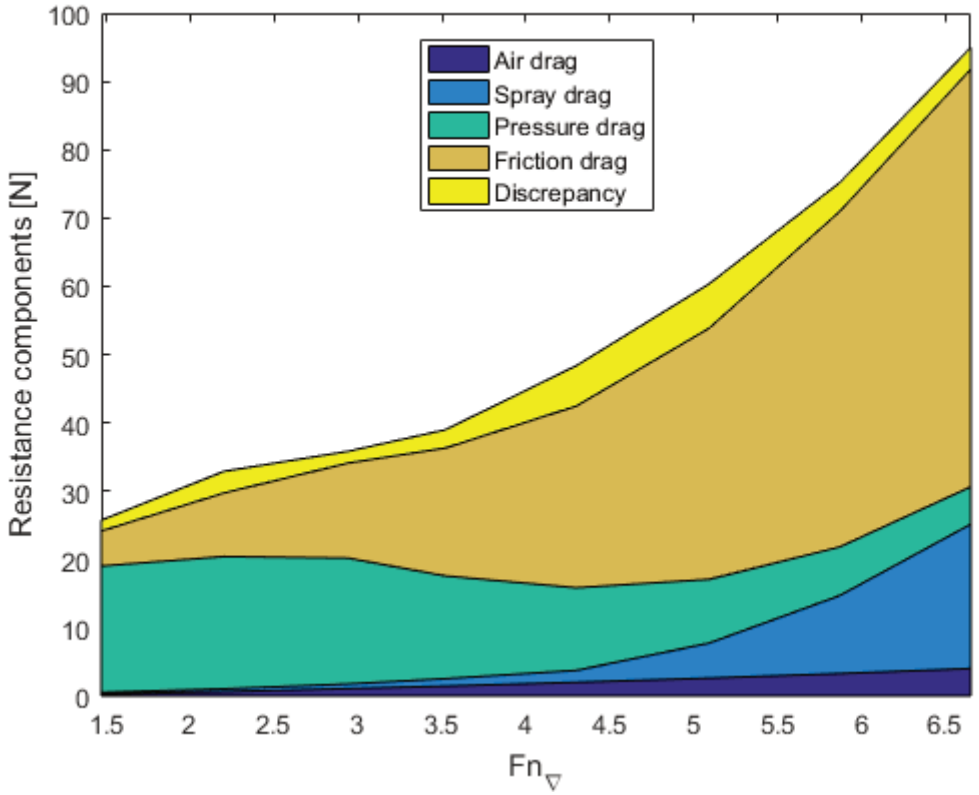

Figure 43. Breakdown of experimental results into force components

Wave runs experimental data

The encounter statistics for the wave runs are shown in Table 14 and the time histories are shown in Figure 44 through Figure 49.

Table 14. Encounter count for the wave runs and average trim values

Hull	Speed [Fn_∇]	Total pitch encounters	Total heave encounters	Average pitch & heave encounters	Average trim	# of runs
Bare hull	1.47	133	96	114.5	5.714	7
Bare hull	4.3	154	96	125	3.372	13
Spray rails	1.47	127	99	113	5.705	7
Spray rails	4.3	152	98	125	3.345	13
Deflector 1	1.47	131	100	115.5	6.456	7
Deflector 1	4.3	148	97	122.5	4.493	13

Bare hull wave tests time history

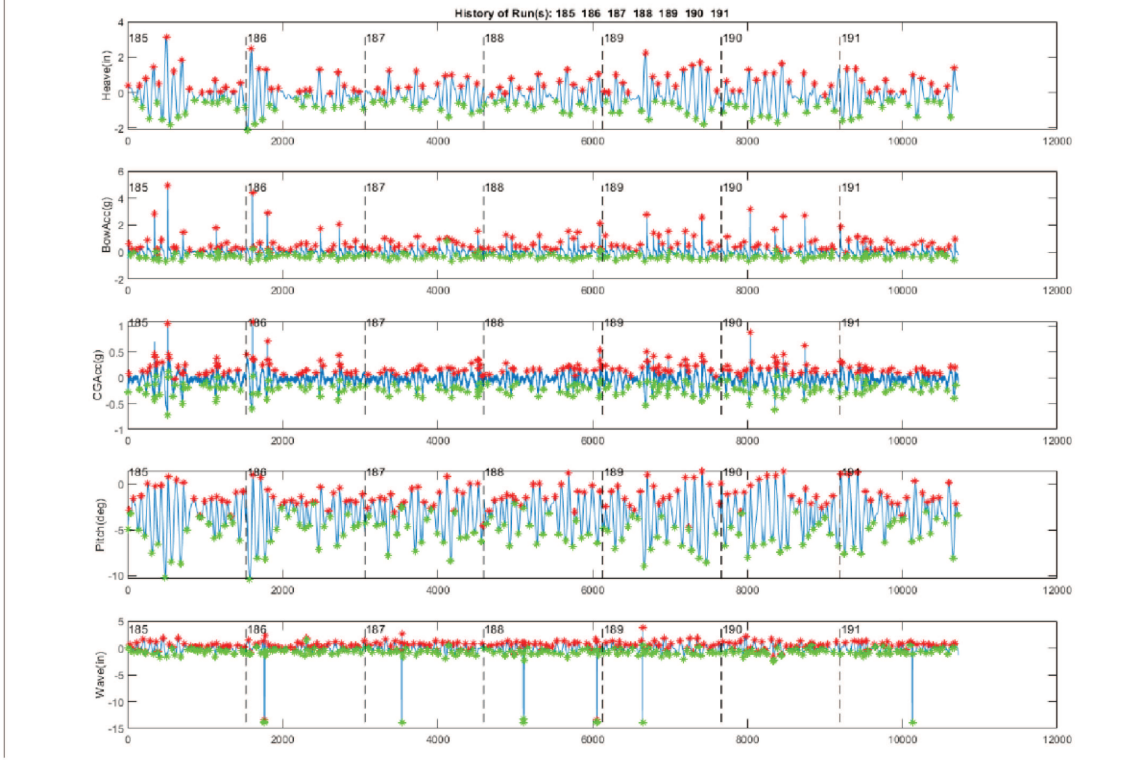

Figure 44. Time history for low speed bare hull

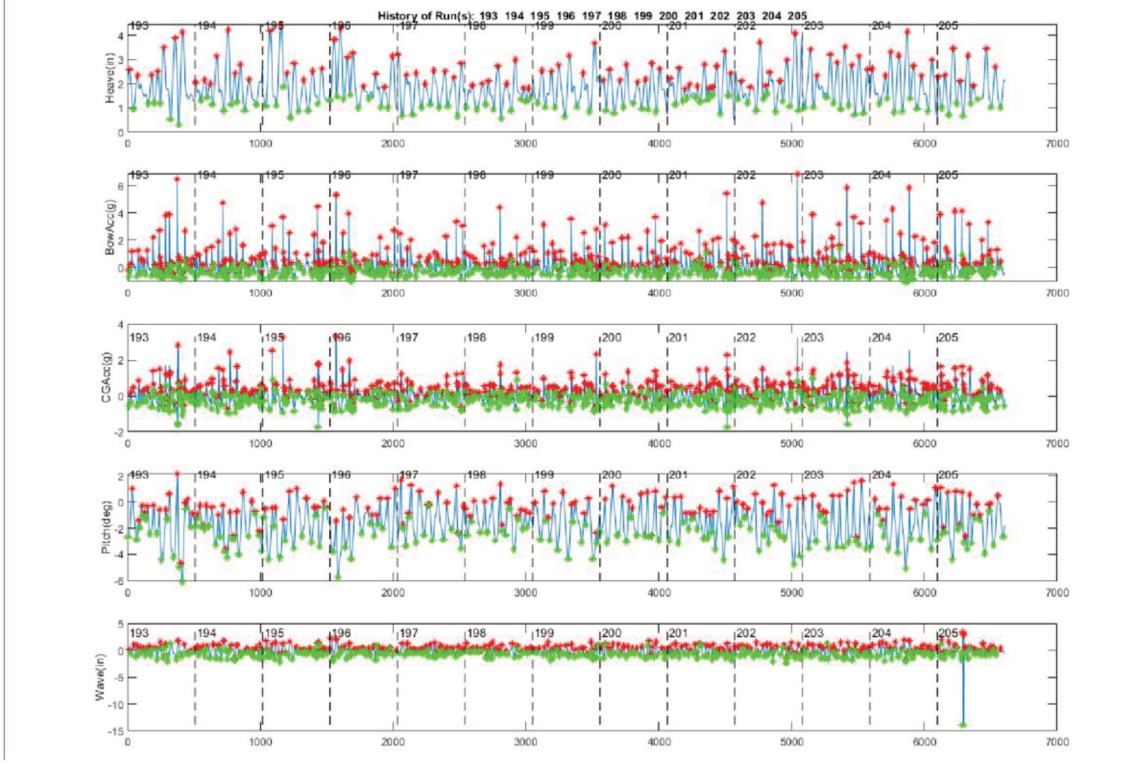

Figure 45. Time history for high-speed bare hull

Spray rails wave tests time history

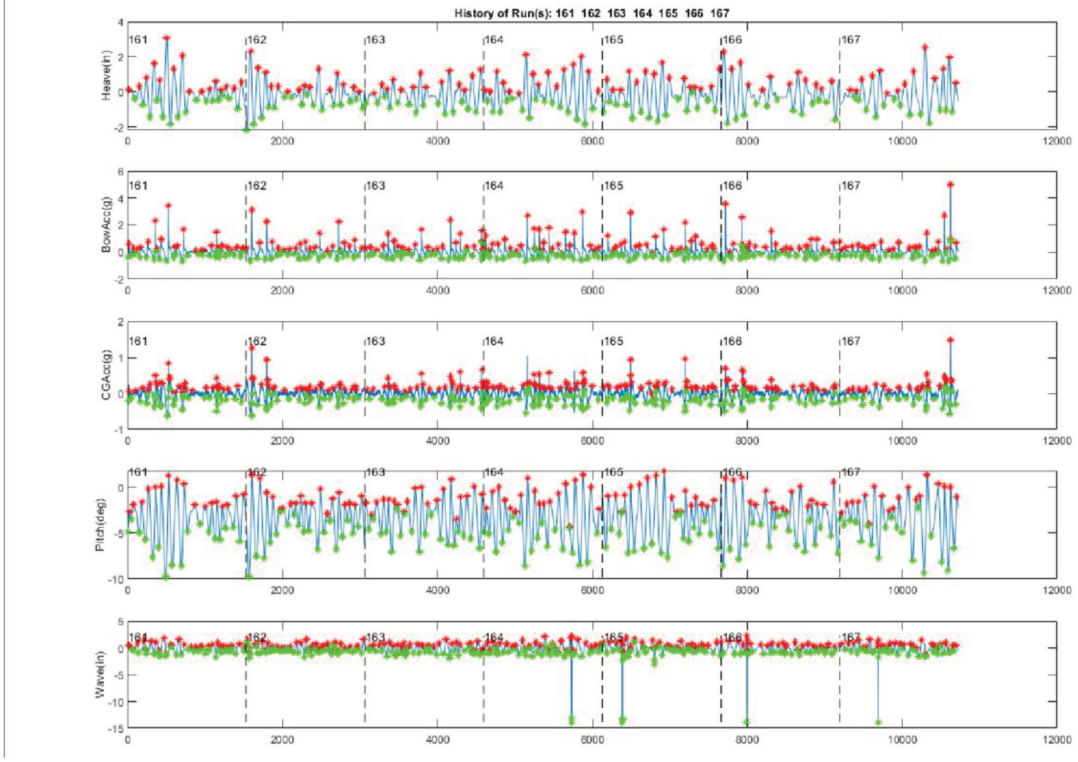

Figure 46. Time history for low-speed Spray rails

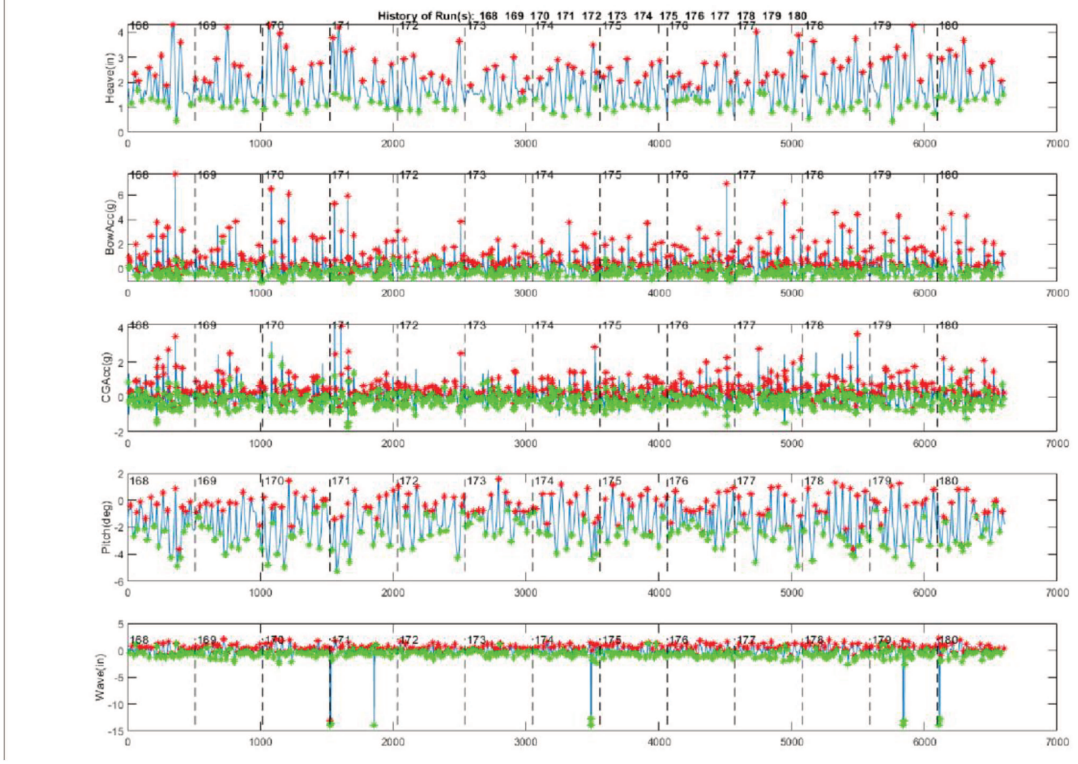

Figure 47. Time history for high-speed Spray rails

Deflectors wave tests time history

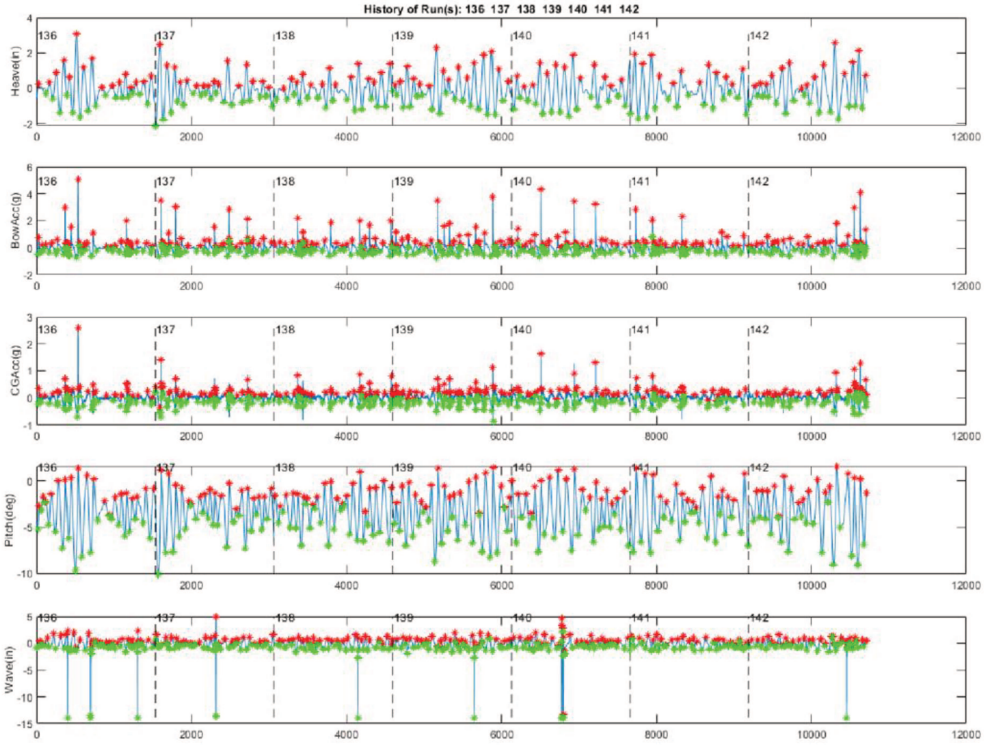

Figure 48. Time history for low-speed Deflector 1

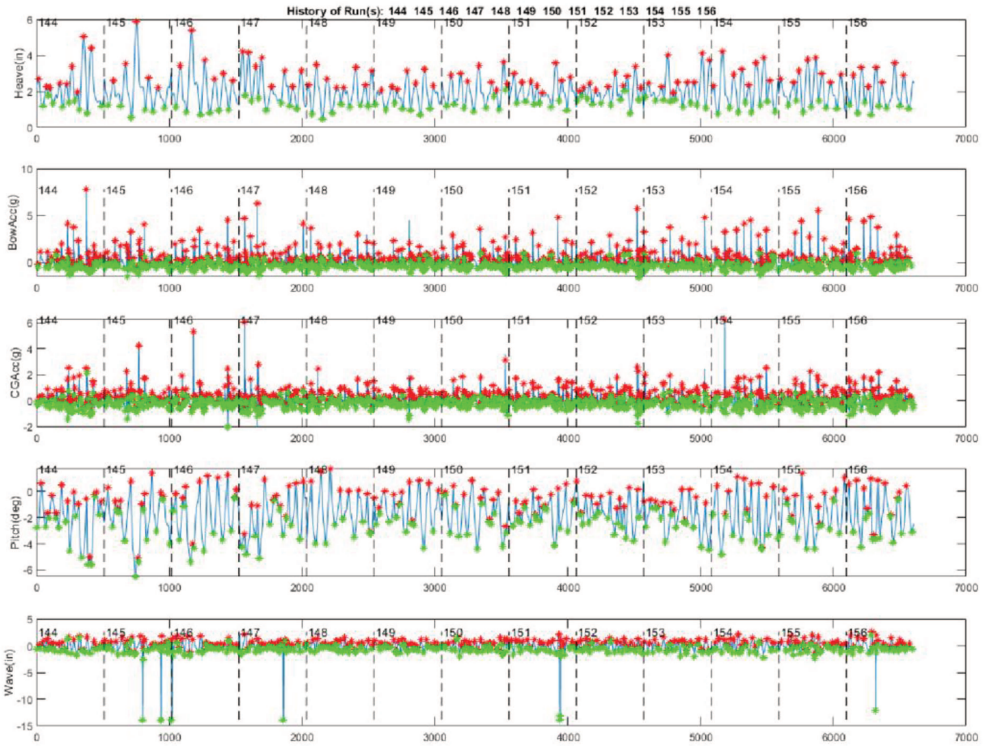

Figure 49. Time history for high-speed Deflector 1